Politecnico di Torino

Ph.D. Dissertation

Electronic Devices

XXVI cycle

Phosphate Optical Fibers for Infrared Fiber Lasers

Emanuele Mura

Supervisors:

Dr. Daniel Milanese

Dr. Joris Lousteau

Table of contents

Chapter 1

Introduction

1.1 Ytterbium fiber laser

The first coherent light emission in a glass was reported in 1961 [1] by demonstrating laser emission in a crown glass doped with neodymium ions. Since then, the progress in the field of fiber laser technology has been enormous and ensured that fiber laser technology today competes strongly with other laser technologies. Thanks to its geometry and efficiency fiber lasers are now becoming an important tool in different fields. including telecommunications, spectroscopy, medicine, materials processing, and military applications. Optical fibers have radically changed the telecommunication industry [2]. Commercial fiber lasers are widely used in medicine [3,4]. Scientific instruments involving spectroscopic investigations of atoms and molecules use fiber lasers as key component. Furthermore, fiber laser technology is widely employed for ranging, remote sensing and security [5]. Fiber lasers with high output power are extensively employed in the materials processing industry. These applications include drilling, micro-machining, marking, cutting and soldering [6]. In particular, for their superior efficiency and versatile fiber lasers are growing rapidly in laser processing industry and they are now competitive with the more traditional gas (CO_2 laser) and solid state lasers (Nd:YAG) [7].

In this industrial area and in particular in marking and precision cutting fields, the key component of many products designed for laser processing is the Ytterbium doped fiber laser in pulsed operation. Operating at wavelengths around 1 μm has some advantages for materials processing compared to the wavelength of about 10 μm typical of CO_2 lasers (e.g. in metal marking). Ytterbium ion is the most ideal rare-element for lasing with only two principal manifolds. Among the different rare-earth ions, Yb^{3+} ion presents a small quantum defect: the absorption wavelengths are close to the emission wavelengths and potentially allowing for very high power conversion efficiencies (>80% optically efficiency), thus reducing thermal effects in high-power lasers. Furthermore, Yb^{3+} ion possesses a broad absorption band in the infrared region of the spectrum, where high power pump diodes are commercial available. One of the key challenges in the development of a powerful high power Yb-doped fiber laser was the injection of the pump light into the small core of low numerical aperture. The solution to overcome this problem was found in the design and the use of double-cladding optical fibers [8,9]. Double cladding optical fibers are made of two waveguides: the core which guides the signal and the first cladding to guide the pump light. In this type of fiber laser, the laser-light propagates in single-mode regime into the core. The core is surrounded by a first, inner cladding in which the multi-mode pump-light propagates. The pump-light is confined inside the inner cladding by an outer cladding with lower refractive index, and also partially propagates into the core where it is absorbed by the laser-active ions. The numerical aperture between inner and outer cladding is high, so that a large number of propagation modes are supported. Therefore, double-cladding fiber lasers can be pumped by multi-mode laser diodes, which have high power but poor beam quality.

Pulsed Yb-doped fiber lasers are commonly based on silica-based glass fibers [10]. In general, the low solubility of rare earth ions in silica forces to use as active medium fiber lengths in the order of meters (typically several tens of meters) to achieve efficient pump absorption. Silica allows to be doped with only few weight percents of rare earth ions (1-2% wt Yb_2O_3) before quenching [11] or photodarkening [12] effects occur. The need of using fiber lengths in the order of meters, together with the low solubility of rare earth ions in silica, causes various problems in the fiber laser system. Main problems are non-linear effects which take place inside the fiber that affect the quality of the output beam and/or the shape of the pulses (e.g. strong broadening of the pulse). The most problematic non-linear effects in high power fiber lasers are: Stimulate Brillouin Scattering (SBS) and Stimulated Raman Scattering (SRS). [13]. SBS refers to the interaction of the optical pulse with acoustic phonons, which can create an acoustic wave that co-propagates with the optical beam along the fiber. The generated acoustic waves reflect part of the incident light in the backward direction. On the other hand, SRS can arise from a transition between two vibrational states in the fiber material, when some of the pump photons are converted into lower-energy photons, and the corresponding part of the optical input energy is shifted to the lattice vibrations. Unlike SBS, both forward and backward Raman scattering are possible. Such non-linear effects are particularly strong for short pulses and they can limit the achievable pulse energies. But in particular non-linear effects critically limit the peak power of the fiber laser [13,14].

There are two possible technological solutions to overcome the SBS and SRS effects. The first solution is the design and the use of large mode area

(LMA) fiber lasers [15,16]. In LMA fiber, the core radius is increased while the numerical aperture (NA) is reduced with the aim of decreasing the optical intensity and thus reduce the non-linear effects. The use of LMA fibers is influenced by technological and manufacturing issues, in fact for single-mode operation the refractive index difference and thus the NA must be very small. Moreover, single-mode LMA fibers, to avoid bending losses which are significant due to the low NA, are difficult to handle and not suitable for compact devices [17].

The second solution to overcome the non-linear effects which occur in high peak power fiber lasers is to increase the doping level of active ions into the core. In fact, in a heavily doped fiber laser the pump power can be absorbed over a small length, and thus short fiber laser that posses high non linear effects thresholds can be used. Since increasing the rare-earth doping level in silica-based fibers is not possible without having deleterious effects such as clustering and quenching, the study and the development of new glass materials as host for rare-earth ions was requested and necessary. Among the different glass systems useful for fiber lasers, phosphate glasses are the most promising. In fact, phosphate glasses allow exceptionally high doping level of rare-earth ions without any concentration quenching, up to 1 x 10^{27} ion/m^3 [18]. An example is reported in [19], where laser emission was obtained from only 8 mm of a phosphate fiber laser doped with 15.8% wt of Yb_2O_3.

In literature several studies demonstrated the large number of attractive properties of phosphate glasses as laser host materials [20-22]. But only few works have focused their attention on phosphate glasses in fiber form and thus

phosphate fiber lasers with an emission at 1 µm in pulsed mode operation [23,24].

1.2 Aim of the work

The main aim of this thesis was to design and manufacture double cladding phosphate fibers doped with Yb ions, suitable as short (cm-level) active cavities in pulsed fiber laser systems.

Starting from the study and the design of novel phosphate glass compositions, it was necessary to fabricate and characterize several sets of glass compositions. Various fabrication methods have been investigated and improved to develop a precise and controlled manufacturing process in order to fabricate high quality and homogeneous phosphate glasses. In fact, phosphate glass is a very reactive and sensitive material: small changes of the manufacture parameters or the type of chemicals caused large variations in the properties on the prepared glass. It was also necessary to study and adjust the different parameters involved in the perform fabrication process to set up a precise and specific method of preforms fabrication by the rod-in-tube technique, with the tubes obtained by rotational casting technique. In particular, a part of this thesis has been dedicated to the design and implementation of a new rotational casting equipment for the cladding tubes manufacture. As a test for the materials and for the different processes, a series of phosphate fibers (active and passive, single and double cladding) were drawn and characterized with the fabricated sets of glasses. Finally laser emission was demonstrated with for the Yb-doped fabricated phosphate fibers.

1.3 Structure of the thesis

This thesis reports the work carried out during my PhD research project and is organized into five chapters, including this introduction.

Chapter 1 introduces the research work fields and the objective of the study. In Chapter 2 the theoretical and technical backgrounds involved in this research are reported. Chapter 2 is divided into two main sections. In the first sections, the principles of optical fiber and fiber laser are explained, with a special focus on the ytterbium ion, the preform fabrication method and the consequent fiber drawing process taken from the literature are also reported and described (from Section 2.1 to Section 2.3). The second part of the chapter is devoted to review phosphate glasses and their structure, with an emphasis on photonic applications of phosphate glasses. Moreover, the state of the art of Ytterbium-doped phosphate glass fibers lasers is given (from Section 2.4 to Section 2.5). In Chapter 3 is reported the experimental work and the methodologies carried out in this research. The different processes and characterization techniques used to fabricate and study the glasses object of this work are presented and explained. The preforms and fiber fabrication processes involved in this work are also described. Chapter 4 reports and discusses the different results on the fabrication and characterization of phosphate glass samples and fibers. The results are divided into five sections: each section involves a different manufactured fiber, with its relative glasses. The last section of the chapter (Section 4.6) describes the results concerning the demonstration of fiber lasers. In Chapter 5 the conclusions and the future developments are reported.

BIBLIOGRAPHY

1 E. Snitzer, “Optical maser action of Nd3+ in a barium crown glass,” in *Phys. Rev. Lett*., vol. 7, pp. 444–446, (1961)

2 R. J. Mears, L. Reekie, M. Jauncey, and D. N. Payne, “Low-noise erbium-doped fiber amplifier operating at 1.54 μm”, in *Electron. Lett.* 26, 1026 (1987)

3 http://surgicalfibers.com/

4 http://www.qioptiq.com/

5 Jeremy T. Dobler ; Michael Braun ; James Nagel ; Valery L. Temyanko ; T. Scott Zaccheo ; F. Wallace Harrison ; Edward V. Browell ; Susan A. Kooi “Applications of fiber lasers for remote sensing of atmospheric greenhouse gases” in *Proc. SPIE 8601, Fiber Lasers X: Technology, Systems, and Applications, 86011Q* (February 26, 2013)

6 http://www.ipgphotonics.com/

7 Nature Photonics, Technology Focus, January 2008

8 R. D. Maurer, “Optical waveguide light source,” U.S. Patent 3,808,549 (1974).

9 H. Po; E. Snitzer, L. Tumminelli, F. Hakimi, N.M. Chu, and T. Haw (1989). "Doubly clad high brightness Nd fiber laser pumped by GaAlAs phased array". In *Optical Fiber Communication Conference. PD7*

10 J. A. Alvarez-Chavez, H. L. Offerhaus, J. Nilsson, P. W. Turner, W. A. Clarkson, and D. J. Richardson, High-energy, high-power ytterbium-doped Q-switched fiber laser” in *Optics Letters*, Vol. 25, Issue 1, pp. 37-39 (2000)

11 Z. Burshtein, Y. Kalisky, S. Z. Levy, P. Le Boulanger, and S. Rotman, “Impurity local phonon nonradiative quenching of Yb3+ fluorescence in Ytterbium-doped silicate glasses,” in *IEEE J. Quantum Electron.*, vol. 26, no. 8, pp. 1000–1007, (2000).

12 Y.-W. Lee, S. Sinha,M. J. F. Digonnet, R. L. Byer, and S. Jiang, “Measurement of high photodarkening resistance in heavily Yb3+ -doped phosphate fibers Yb3+ -doped phosphate fiber laser,” in *Electron. Lett.*, vol. 44, no. 1, pp. 14–16, (2008).

13 K. Okamoto Fundamentals of Optical Waveguides, Academic Press (2006).

14 M.J. Digonett, Rare-Earth-Doped Fiber Laser and Amplifier, Marcel Dekker, Inc., (2001).

15 M. E. Fermann, “Single-mode excitation of multimode fibers with ultrashort pulse, in *Optics Letters*, 23-1, 52-54 (1998).

16 http://www.nktphotonics.com/lmafibers

17 J. Limpert, A. Liem, M. Reich, T. Schreiber, S. Nolte, H. Zellmer and A. Tünnermann, in *Optics Express*, 12-7, 1313-1319 (2004)

18 S. Xu, Z. Yang, W. Zhang, X. Wei, Q. Qian, D. Chen, Q. Zhang, S. Shen, M. Peng, and J. Qiuet “400 mWultrashort cavity low-noise single-frequency Yb3+-doped phosphate fiber laser” in *Optics Letters*, 36(18), 3780-3710 (2011).

19 D. L. Veasey, D. S. Funk, P. M. Peters, N. A. Sanford, G. E. Obarski, N. Fontaine, M. Young, A. P. Paskin, W. Liu, S. N. Houde-Walter, J. S. Hayden, “Yb/Er-codoped and Yb-doped waveguide lasers in phosphate glass” in *Journal of Non-Crystalline Solids* 263&264, 369-388, (2000).

20 C. Florea and K. A. Winick, “Ytterbium-Doped Glass Waveguide Laser Fabricated by Ion Exchange” in *Journal of Lightwave Technology*, 17(9), (1999).

21 L. I. Avakyants, V. I. Molev, A. E. Pozdnyakov and V. F. Surkova, “A new phosphate laser glass” in *Journal of Optical Technology*, 71(12), 828-829, (2004).

22 M. Leigh, W. Shi, J. Zong, J. Wang, S. Jiang and N. Peyghambarian, “Compact, single-frequency all-fiber Q-switched laser at 1 μm” in *Optics Letters*, 32(8), 897-899, (2007).

23 H. Chen, G. Chang, S. Xu, Z. Yang and F.X. Kärtner, “3 GHz, fundamentally mode-locked, femtosecond Yb-fiber laser” in *Optics Express*, 37(17), 3522-3524 (2012).

Chapter 2

Backgrounds

In this chapter, the optical fiber (Section 2.1) and the operation principles of the fiber laser (Section 2.2) are described, giving particular attention to ytterbium ion emission. In Section 2.3, the preform fabrication method and the consequent fiber drawing process are described.

2.1 Optical Fiber

Optical fibers, which form the gain medium in fiber lasers, are basically waveguides for electromagnetic radiation at optical frequencies [1]. An optical fiber is a cylindrical structure made of glass that is made of a ***core*** layer of diameter ***a*** and refractive index n_1, and a surrounding ***cladding*** layer of diameter ***b*** and refractive index n_2. See Figure 2.1.

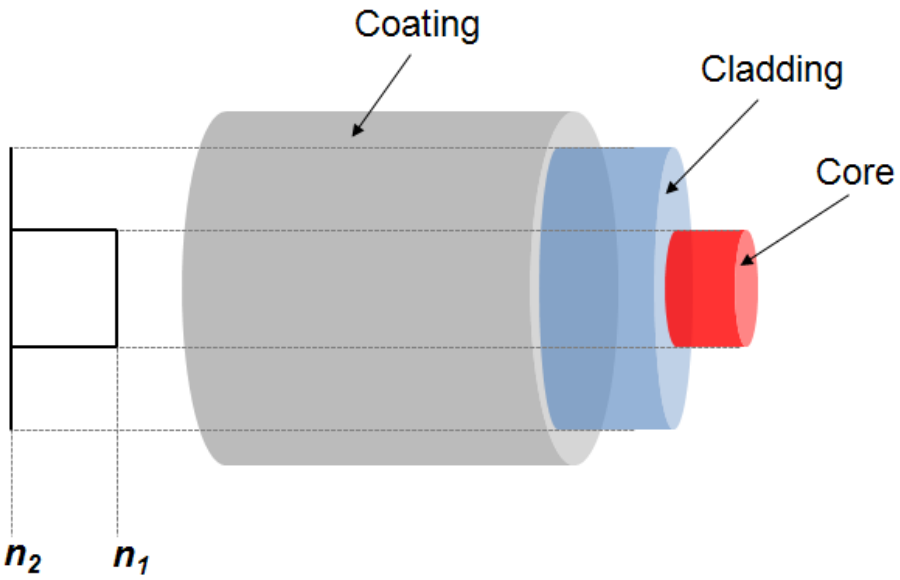

Figure 2.1: Schematic of an optical fiber and its transverse refractive index profile

The structure can also be surrounded by a polymer coating with a refractive index $\boldsymbol{n_3}$ lower than n_2. The basic function of the polymer coating is to maximize the fiber strength and to protect the inner layers against micro-bending.

Light is guided in the core by ***total internal reflection*** at the core/cladding interface. In particular, the refractive index of the cladding $n_2$must be lower than the refractive index of the core n_1 in order to confine and guide the light inside the optical fiber. Not all source radiation can be guided over the optical fiber[1]. Only rays falling within a specific solid angle or “cone” at the input of the fiber can typically be propagated through the fiber. The maximum angle at which an incident ray can be coupled into the fiber core can be determined by the refractive indexes of the core n_1 and the cladding n_2. In particular, the sine of this maximum acceptance angle is the ***numerical aperture*** (NA), and it is a

characteristic parameter of optical fibers. The numerical aperture of an optical fiber can be calculated from the index difference as follows [1,2]:

$$NA = \sqrt{{n_1}^2 - {n_2}^2} \qquad (2.1)$$

Other important properties of an optical fiber are related with guided modes, which are primarily governed by the waveguide structure and materials. Fibers can be classified indeed into two main categories: ***single-mode*** and ***multi-mode*** fibers [1-3]. The number of modes supported by the fiber is definite by the normalized frequency or the so-called ***V-number*** which is a function of the numerical aperture of the fiber [1]:

$$V = \frac{2\pi NA}{\lambda} \qquad (2.2)$$

where ***a*** is the core radius and ***λ*** is the wavelength of the propagating light in vacuum. The simplest type of fiber is the single-mode (SM) fiber, in which the core size and refractive index difference are small, allowing only the fundamental mode to be propagated. A single mode fiber is characterized by values of V-number lower than 2.405, meaning that for higher values of V-number the fiber becomes multi-mode. The core radius of a single-mode fiber is usually in the range of 3 to 8 µm, depending on the operating wavelength. While, in multi-mode fiber the core radius is much higher, typically from 25 to 50 µm [1,3].

2.2 Optical Fiber Laser

C. J. Koester and E. Snitzer [4] in 1964 described the first coherent light emission in a multi-component glass fiber. Today's fiber laser technology is an established technology and undergoing expansion and growth. Fiber laser is a particular kind of solid-state lasers but, rather than simply being manufactured in the form of a bar or a slab, is produced into fiber form. The main advantages that make the fiber laser interesting and competitive with other types of laser are [5, 6]:

- *Good heat dissipation*, due to the intrinsic high surface area to volume ratio, which allows efficient cooling;
- *High efficiency*, 25-30% measured as the fraction of the electrical power input that emerges as laser power output (e.g. CO_2-laser, it is in the order of 15-20%);
- *Remote delivery*, the laser beam can be directed and focused to movable elements simply by properly orienting the fiber end. This is important for laser cutting, welding, and folding applications;
- *Compact size*, fiber can be bent and coiled to save space;
- *Low cost*; the manufacturing processes are easier and less expensive compared to other solid state laser systems or gas lasers.

Fiber lasers are now widely used in many applications, included telecommunication, material processing, spectroscopy, medicine and military applications. Fiber lasers with high output power are extensively employed in materials processing applications. These applications include drilling, micro-machining, marking, cutting, welding and soldering [7]. Fiber lasers find an

important application in the field of medicine. The features of fiber lasers are well-suited for endoscopic and/or surgical procedures, such as tracking tumors [8,9]. Fiber lasers are used in a variety of scientific fields involving spectroscopic studies of atoms and molecules [10]. Moreover, fiber laser technology is widely used for ranging, remote sensing and security [11,12].

2.2.1 Principles:

a) Rare-Earth doped Laser

Fiber lasers are generally based on optical fibers (active medium) doped with rare-earth (RE) ions. Rare earths are characterized by the progressive filling of the 4f orbitals. The internal electronic structure $5s^2 5p^6 6s^2$ is the same for each atom of this period. The spectroscopic properties of the different rare-earth ions therefore depend on the number of electrons present on 4f level: the spectra in the infrared, visible and in some cases also in the ultraviolet region are dictated by transitions between 4f levels.

A RE ion during a pump process is excited from its initial state $\boldsymbol{E_g}$ (ground state), by absorption of a pump photon of energy

$$E_1 = h_p \nu_1 \qquad \textbf{(2.3)}$$

to a higher energy level $\boldsymbol{E_h}$, where $\boldsymbol{h_p}$ is the Planck constant, and $\boldsymbol{\nu_1}$ is the frequency of the photon. From the excited state E_h de-excitation to the ground state $\boldsymbol{E_g}$ can take place either by ***spontaneous*** or ***stimulated emission***, and in both cases a photon of energy $E_3 = E_m - E_g$ is emitted. If the ion spontaneously decays, the photon is emitted with random phase and direction. In stimulated

emission, on the contrary, an incoming photon with energy E_3 promotes de-excitation of the ion from the upper lasing level E_m, with the creation of a photon having the same properties of phase, polarization and direction as the incoming photon, and thus leading to amplification of light.

Depending on the ion and the pump wavelength, the lasing process can result in a different scheme, but it can be usually simplified to a three or a four or a quasi-three level laser scheme (see Figure 2.2) [5].

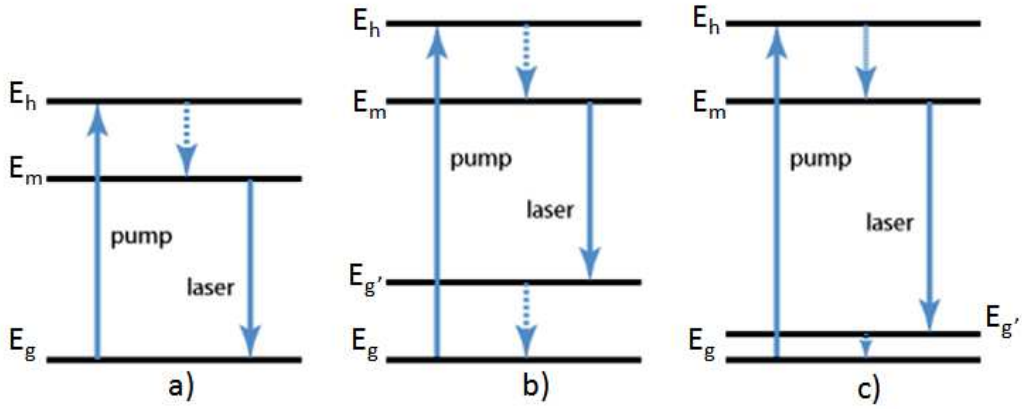

Figure 2.2: a)Three-level lasing scheme; b)Four-level lasing scheme; c) a quasi-three level lasing scheme

Figure 2.2 shows the schemes of the different lasing processes. When the ion is relaxed directly from E_m level to the E_g level, the process follows a three level lasing scheme (see Figure 2.2-a), which takes place for example in the case of the ruby laser (Cr^{3+}:Al_2O_3) [13]. Differently, the ion can be de-excited to another level ($E_{g'}$), from which it relaxes non-radiatively to the ground state thus concluding a four level lasing process (Figure 2.2-b). The most popular four-level solid-state gain medium is the Nd:YAG laser [14]. There exists the possibility of

an intermediate situation: a quasi-three level scheme (see figure 2.2-c). In a quasi-three-level laser medium the lower laser level is so close to the ground state that an appreciable population in that level occurs in thermal equilibrium at the operating temperature. Examples of quasi-three-level media are all ytterbium-doped gain media (e.g. Yb:YAG, or Yb:glass as used in optical fibers) [15]. However, pronounced three-level behavior is inevitable for gain media with a very small quantum defect, because this enforces small energy spacing between the lower laser level and the ground state, so that thermal population of the lower laser level is significant. In a three level scheme, absorption from the ground state to the upper lasing level with energy E_m can occur, provoking reabsorption of emitted photons. As a consequence, in order to achieve gain, higher levels of pump power are required. This is not the case in lasers following a four level scheme, which benefit from having lower values of threshold powers (e.g. Nd^{3+}:glass and related fibers lasers).

An important parameter in the study of rare earth ions as active elements for lasers is the **cross section** of the ions [1,6]. The cross section represents physically *the probability that an interaction between a rare-earth ion and a photon of a λ wavelength, which propagates in the medium, takes place.* Since the active medium interacts with the photons both during pumping (absorption process) and both during the emission, two distinct cross-sections can be defined: ***absorption*** and ***emission***. Thus, the amounts of absorbed and emitted light power at a given frequency can be defined as:

$$P_{a,e} = \sigma_{a,e} I \qquad \textbf{(2.4)}$$

where the absorption and emission cross sections are respectively $\boldsymbol{\sigma_a}$ and $\boldsymbol{\sigma_e}$ (in units ofm^2), and ***I*** is the incident light intensity (in units of W/m^2). Moreover, absorption and emission cross sections are dependent on the host glass and the magnitude of the deviations from one host to another was observed to be up to about 30% [15]. In Figure 2.3 the absorption and emission cross sections of Yb^{3+}in aluminosilicate glass are reported [16].The absorption cross section can be easily calculated from UV-Vis spectroscopy measurements (see Section 3.2.4).

Another important parameter in the study of rare earth ions is the ***upper-state lifetime***. In a laser gain medium, lasing is associated with the population of an excited state, from which stimulated emission can occur. In general, the lifetime of this level is define as *the time after which the population of the excite state-level has decayed to 1/e (around 1/3)* and it is inversely proportional to the probability per unit time of the exit of a ion from that excited level. The usefulness of lifetime lies in the possibility of quick comparison between the various phenomena, intended and unintended, which may occur in the active medium. A long radiative lifetime in a laser gain medium is preferred because a significant population inversion can be maintained with a relatively low pump power [1,5].

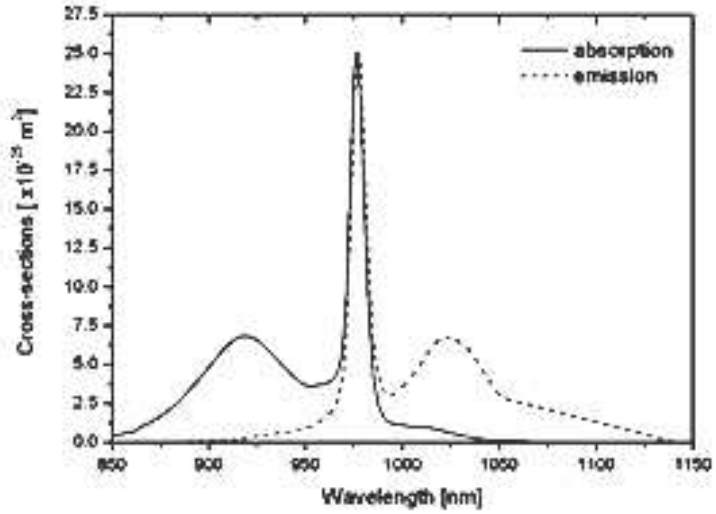

Figure 2.3: Absorption and emission cross sections of ytterbium in an aluminosilicate glass [16]

The wavelengths of pump absorption and signal emission for a laser system depend on the energy level arrangement of the rare earth ions in the host glass. Table 2.1 summarizes the main laser active RE-ions with their common host glasses and emission wavelengths appearing in order of importance

Table 2.1: Rare earth ions and common host glasses related with emission wavelengths

RE ion	***Host glass***	***Emission wavelengths (µm)***
Yb^{3+} *Ytterbium*	*silicate phosphate*	*1.00-1.10*
Er^{3+} *Erbium*	*silicate phosphate fluoride*	*0.55; 1.5-1.6; 2.7*
Nd^{3+} *Neodium*	*silicate phosphate*	*0.9; 1.03-1.10; 1.32*

The most interesting rare earth ions used as dopants in optical fibers are Neodymium (Nd), Erbium (Er) and Ytterbium (Yb) for emission in the near infrared wavelength region [5]. Nd^{3+} ions have an emission at around 1080 nm, and can be pumped at around 800 nm [17]. Neodymium was one of the first dopants to be incorporated into fiber [18]. However, in terms of energy the efficiency of Nd^{3+} is low, and as a consequence it has been replaced by Yb^{3+} as the dopant of choice for high-power fiber lasers. Er^{3+} ions have an emission at wavelength at around 1550 nm and are the very popular for the telecom applications of the EDFA (erbium-doped fiber amplifier) [19,20]. Glasses doped with Er^{3+} ions can be sensitized by adding Yb^{3+} ions [21]. This co-doping allows the fiber to be pumped within the Yb^{3+} absorption band and subsequently exploit the energy transfer to the Er^{3+} ions. On the other hand, Yb-doped fiber lasers are the key component of the modern high power lasers [7].The emission wavelength of Yb^{3+} ions is around 1060 nm when pumped at around 970 nm [6] and further details of this ion will be provided in the following section.

b) The Ytterbium ion

Ytterbium has become a very important RE-ion for high-power applications due to its high pump-to-signal energy conversion efficiency around 1 µm [7].The energy level diagram, of Yb^{3+}ions, if compared to other RE ions, has a simple structure consisting of two well-separated levels or manifolds: the ground state $^2F_{7/2}$ and the excited state $^2F_{5/2}$. These two levels are split further into several sub-levels (Stark levels) [22].The upper ($^2F_{5/2}$) and the lower ($^2F_{7/2}$) levels have three and four Stark levels respectively. Laser transitions can take place between different combinations of sub-levels in the two manifolds, due to

the Stark splitting. The corresponding transitions between the sub-levels are not discrete energy levels because of homogeneous and inhomogeneous broadening in the glass at room temperature. In fact, Ytterbium ions offer a broad absorption band that extends from 850 nm to 1040 nm [6]. Consequently, the pump wavelengths can be selected from a broad range of wavelengths(see Figure 2.4).

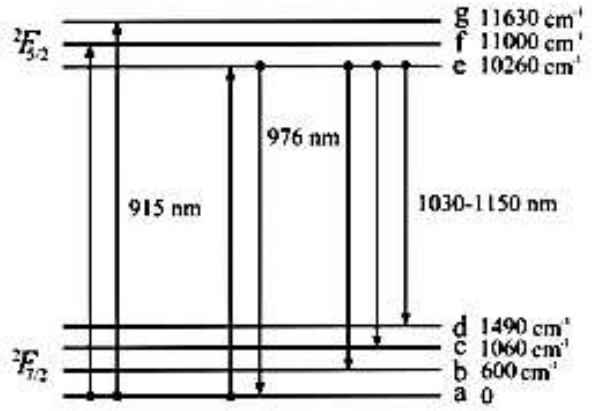

Figure 2.4: Energy level diagram illustrating the ytterbium ground $^2F_{7/2}$ and excited $^2F_{5/2}$ levels and possible transitions between the sub-levels[22]

However, ytterbium ions exhibit strong absorption and emission peaks at975 nm, corresponding to the transition between sub-levels ***a*** and ***e***. Those levels are the most thermally populated sub-levels according to the Boltzmann's distribution, and thus, represent the most probable transition. In Yb-doped fiber, pump signal at 975 nm is then preferred due to the high pump absorption of Yb^{3+} ions at this wavelength. The radiative lifetime of the $^2F_{5/2}$ level, depending on the

host, is usually in the range of 1.0 to 1.4 ms [23]. Another well-known advantage of the simple Yb^{3+} energy level diagram is the absence of higher energy levels (see Figure 2.4). This absence significantly reduces the multi-phonon relaxation and ESA processes and, therefore, eases the development of high-power lasers. Moreover, the high absorption and emission cross sections of Yb^{3+} ion [24] allow for very strong pump absorption and very short fiber lasers.

c) Double-Cladding Optical Fiber

Double-clad optical fibers (DCOF) are an important technological solution in the field of high-power fiber lasers. Instead of the classical two layer (core/clad) structure, double cladding fibers are made of a structure of three concentric layers: core, inner cladding and external cladding. The refractive index profile decreases from the core to the second, external cladding [25,26]. In Figure 2.5 a scheme of a double-cladding fiber is shown.

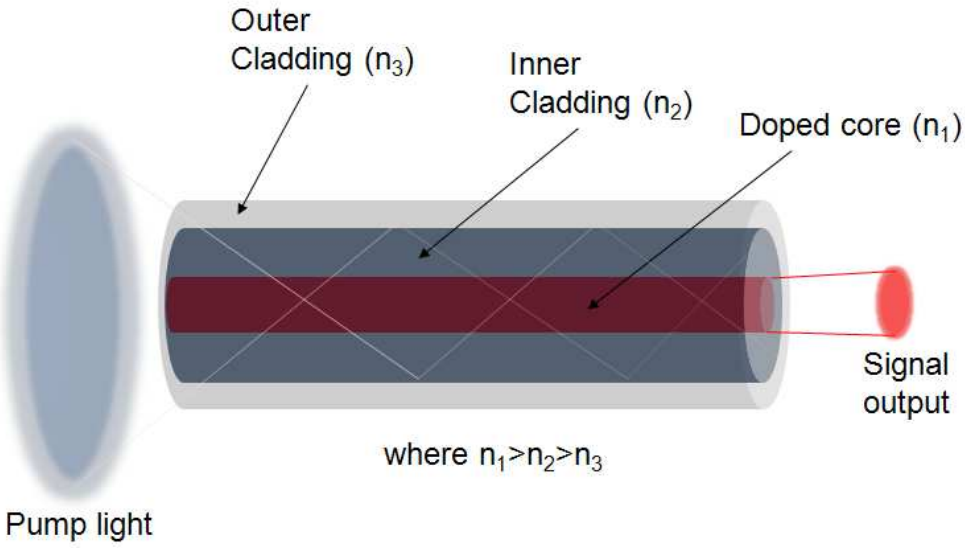

Figure 2.5: Illustration of a double cladding fiber laser and its transverse refractive index profile

In DCOF, the laser light is confined and is propagated into the fiber core which is doped with active ions. Surrounding the core region is the inner cladding, into which the pump light is launched and confined in a multi-mode regime. The pump light is confined inside the inner-cladding region thanks to the lower refractive index of the second cladding and gradually absorbed by the active ions in the core as it propagates. The area of the inner-cladding in a double-cladding fiber is significantly larger than that of the core, and therefore supports many modes.

The pump light, in conventional fiber laser, is coupled into the fiber core (core-pumped), which imposes limitations on the maximum pump power available. In fact, efficient coupling of the laser diode output into the single-mode fiber core needs the use of a single-mode laser diode. The output power of laser diodes is however limited by the damage threshold of the semiconductor material

to a fraction of a watt, which limits drastically the maximum output power of the fiber laser [5]. On the other hand, double-clad fibers that are cladding-pumped combine the high power conversion efficiency with the high beam quality [25-29]. DCOF converts low intensity pump light into a high brightness signal light. In fact, double-cladding fibers, that were developed to allow high-power multimode diodes with low beam quality to be used for the pump light, can also be seen as a brightness converter [27,28]. The energy level of these pump diodes have been increasing very steeply in the past decades. Nowadays, single-emitter pump diodes can give ~50 W of output power while the multi-emitter bars can go up to ~500 W. However, coupling such high power into a single-mode fiber core is impossible: output of these diodes can only be coupled into fibers with core diameters ranging from 105 μm to 600 μm depending on the power level. For a single-mode fiber, it is only possible to couple around 1 W. The only way to increase coupled power is to increase the core diameter. However, there is a practical limit for the core diameter if a single-mode laser operation is desired: a larger core requires a low NA between core and cladding and fabricating a preform with a *NA* below ~0.05 is quite challenging. Below this value, the fibers become very sensitive to the bending losses, and the splice losses also increase. These problems are overcome by using double-cladding optical fiber, that can be pumped by high-power multimode diode with poor beam quality.

The ratio of the areas of inner cladding and core is an important parameter to take into account at the design stage of the double cladding fiber. This area ratio should not be too large, because otherwise the effective pump absorption length becomes large, and the pump intensity in the core is small, resulting in low excitation levels which can also compromise the power efficiency. Area ratios of

the order of 100–1000 are common [30]. Pump sources with improved brightness allow the use of fibers with a smaller area ratio, and thus also with a smaller length, which also reduces the impact of various types of nonlinearities.

d) Attenuation losses

When propagated along the fiber, the light is attenuated and propagation loss occurs. The reduction of intensity of the light beam (or signal) as it travels along the fiber is mainly caused by absorption and/or scattering phenomena, and they are usually expressed in dB/m units [1-3]. The origin of the attenuation losses can be divided into extrinsic and intrinsic.

Intrinsic losses are material dependent and some of the energy from the propagating wave is converted to other forms of energy, for example, heat by generation of lattice vibration. These phenomena can occur both because of electronic transitions (in the UV region of the spectra) and vibrational resonances (due to the IR absorption)and their overtones (extending into the NIR region). Also the microscopic variation on the structure of the glass, in which the refractive index is different than the medium, can cause intrinsic losses by Rayleigh scattering. That loss is proportional to the inverse 4th power of the wavelength. It usually dominates the loss at visible and near-infrared wavelengths [31,32].

On the other hand, ***extrinsic*** losses are additional losses due to imperfections that could in principle be avoided. Extrinsic absorption losses can be caused by unwanted impurities. Among the most important source of impurities are the hydroxyl groups and transition metals that in the near infrared wavelength region [31,32]. These can be minimized by improving the method of

fabrication. Moreover, extrinsic scattering can be due small particles present inside the optical fiber. The result is that this local change acts like a small dielectric particle and scatters the propagating light in a different direction. Also, rough and irregular surfaces or irregular core/cladding interface, can cause scattering of light rays in optical fiber [31,32].

e) Pulsed mode operation

A laser can be classified as operating in either continuous or pulsed mode, depending on whether the power output is essentially continuous over time or whether its output takes the form of optical pulses. The pulsed laser can still be divided according to the pulses duration: short (generally nanoseconds) or ultashort pulsed (picoseconds or femtosecond) lasers.

A common technique to obtain short pulses from fiber lasers is the ***Q-switching*** technique [31,33]. The generation of a Q-switched pulsed laser can be described as a reduction of the quality factor or 'Q' of the cavity. The operation principles can be described as follows. The resonator losses are initially kept at a high level. As lasing cannot occur at that time, the energy fed into the gain medium by the pumping process can be stored in the active fiber. Then, the losses are suddenly reduced to a small value, so that the power of the laser radiation builds up very quickly in the laser resonator. The resulting pulse can extract much of the stored energy. The loss switching may be accomplished actively or passively.

For ***active*** Q-switching, the losses are modulated with an active control element, typically either an acousto-optic or electro-optic modulator[33]. Here, the pulse is formed shortly after an electrical trigger signal arrives. In any case, the

achieved pulse energy and pulse duration depends on the energy stored in the gain medium, i.e. on the pump power and the pulse repetition rate. For ***passive*** Q-switching, the losses are automatically modulated with a saturable absorber [34,35]. In this case, the pulse is formed as soon as the energy stored in the gain medium (and thus the gain) has reached a sufficiently high level. In many cases, the pulse energy and duration are then fixed, and changes of the pump power only influence the pulse repetition rate. Typical applications of Q-switched lasers are material processing (e.g. cutting, drilling, laser marking), pumping of nonlinear frequency conversion devices, range finding, and remote sensing [36,37].

Ultrashort pulses, with durations measured in picoseconds or in femtoseconds, can be generated with ***mode-locked*** fiber lasers [32,38]. In this kind of technique, one or several ultrashort pulses circulate in the resonator, and each time such a pulse hits the output coupler, a pulse is emitted. Within each resonator round trip, a pulse is subject to various effects, but its parameters stay approximately unchanged after each round trip. In contrast to typical solid-state bulk lasers, ultrashort pulses in a fiber laser resonator experience strong dispersive and nonlinear effects in each round trip, because such effects are much stronger in a fiber than in a short crystal and in air. When very short pulses, high pulse energies, and high peak powers are wanted in particular, however, nonlinear and dispersive effects are often much stronger than desirable, and limit the achievable performance.Such mode-locked lasers find interesting application for researching processes occurring on extremely short time scales [39], for maximizing the effect of nonlinearity in optical materials (e.g. in second-harmonic generation) due to the large peak power [40], and in ablation applications [41].

2.3Fiber Fabrication Process

2.3.1 Preform Fabrication

Standard optical fibers are obtained by assembling first a large-diameter preform, with a carefully controlled refractive index profile, which is then pulled to form the long, thin optical fiber. There are several methods to produce a preform, which can be divided in: processes via vapor deposition and processes via melting technique.

a) Vapor Deposition

Chemical vapor deposition (CVD) is the most common technique for silica preform manufacturing [33]. As shown in Fig. 2.6, gaseous solutions of silicon chloride ($SiCl_4$), germanium chloride ($GeCl_4$) and/or other chemicals are mixed and bubbled with oxygen. The precise mixture governs the various physical and optical properties (refractive index, coefficient of expansion, glass transition temperature, etc.) of the final preform. The gas vapors are then passed through a rotating silica glass tube or quartz tube (cladding) in a special lathe, which is heated up to ~1600 ℃ with a burner that continuously moves back and forth.

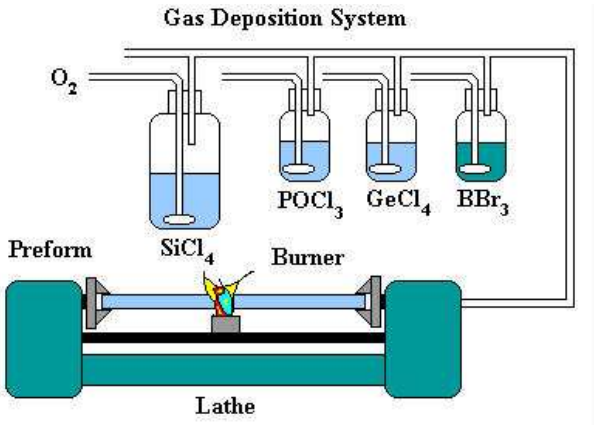

Figure 2.6: Scheme of the chemical vapor deposition process [42]

Here, $SiCl_4$ is oxidized and form fine soot of silica, which coats the inner surface of the glass tube near the burner and is sintered into a clear glass layer. Other dopants can be included to the process for changing the index (Ge, P, B, F) and creating an active lasing medium (Rare-earths like Yb, Er, etc.). Finally, the tube is collapsed by heating it up to 2000 ℃.

Different techniques have been developed based on the CVD principle. ***Outside vapor deposition*** (OVD) is a process where the silica soot is deposited on the surface of some target rod (e.g. a glass mandrel), rather than inside of a tube as with CVD. ***Vapor phase axial deposition*** (VAD) is similar to OVD, but uses a modified geometry, where the deposition occurs at the end of the target rod so long performs can be made. ***Plasma chemical vapor deposition*** (PCVD) uses deposition inside a tube, similar to CVD. However, instead of a burner, microwaves are used for heating the deposition region. The deposition is slow, but very precise [33,43-45].

b) Melting Process

Various fabrication techniques are used to manufacture preforms via melting process. In the ***extrusion*** process, the core melt is pressed into the cladding melt. The core glass is above the cladding in a sleeve. Both are heated until the softening glass temperature and a pressure is applied. A cane with a core-clad structure is extruded as shown in Figure 2.7. The extruded cane is used as a core-clad preform [46].

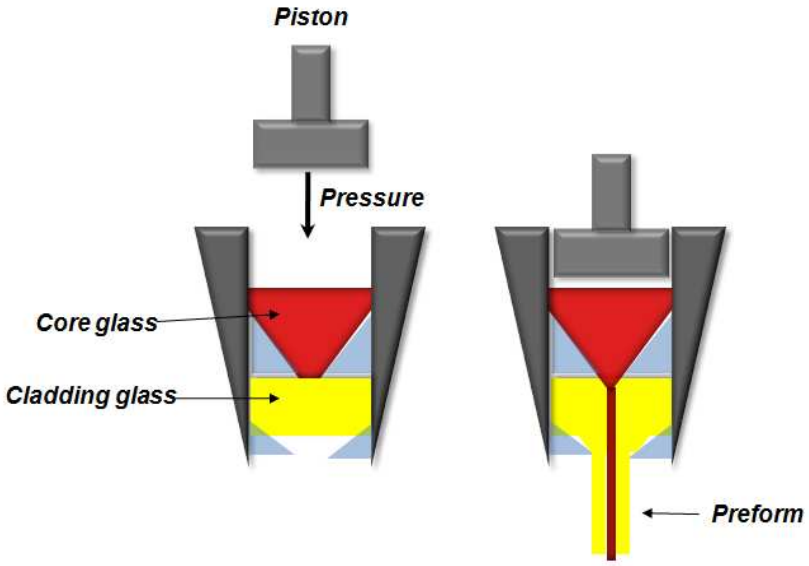

Figure 2.7: Scheme of the extrusion process

In the ***built-in-cast*** process, the cladding-glass is first quenched in a mold pre-heated at around the glass transition temperature and immediately turned over. Then, the core melt is cast inside the cylindrical hollow in the middle of the mold. This process has been specially developed for fluoride glass performs fabrication. In Figure 2.8 the 3 steps of the process [47] are shown.

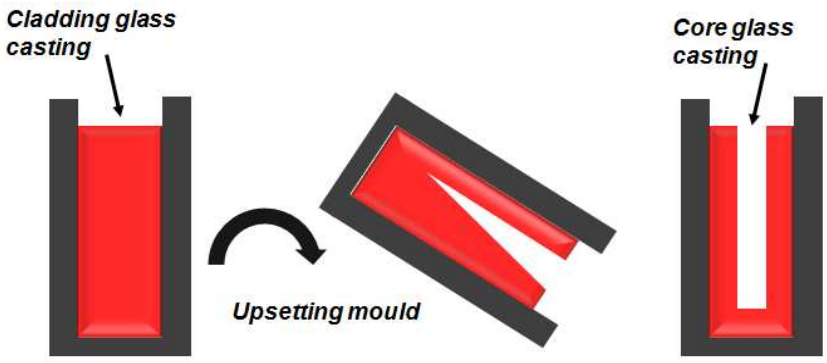

Figure 2.8: Scheme of the built-in-cast process

The ***rod-in-tube*** process is based on the individual preparation of the core and the cladding components. This technique consists in matching the core rod into the cladding tube (see Figure 2.9). The cladding tube can be obtained from glass rod drilled through its center [48] or directly from the melt by rotational casting [49].

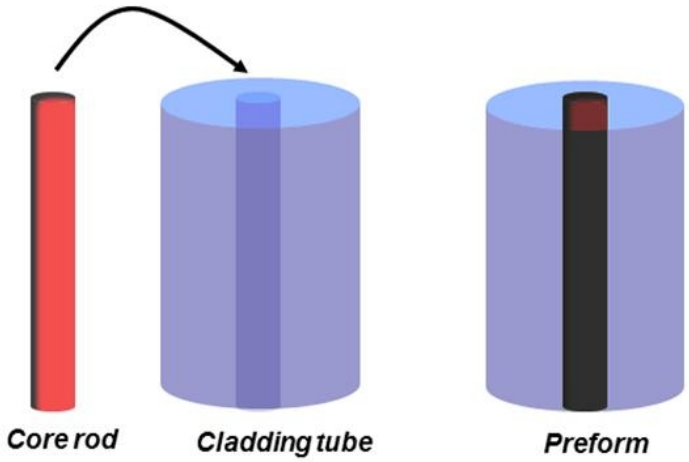

Figure 2.9: Scheme of the rod-in-tube process

2.3.2Fiber Drawing Process

The second stage of fiber production is to convert the glass preform into fiber using a drawing tower. The configuration and specification of the fiber-drawing equipment (Fig. 2.10) depend on whether it is designed for industry or research, while the basic components are essentially the same.

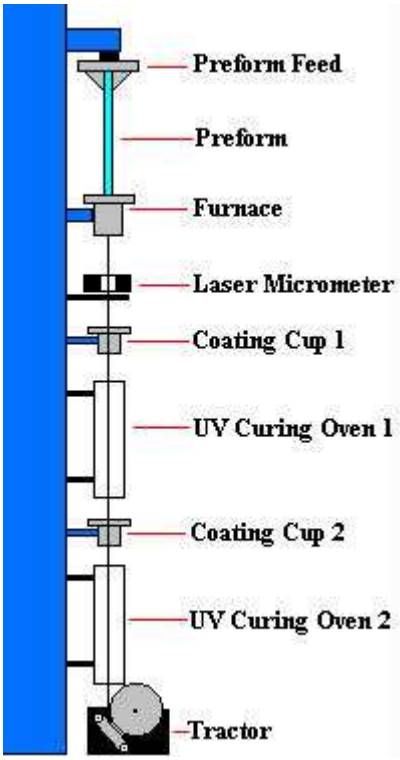

Figure 2.10: Scheme of a drawing tower [42]

The major difference is that in commercial equipment, where hundreds of kilometers of fiber can be produce every day, the drawing speed can be in excess of 600 m/min. As the maximum drawing speed required increases, the height of the tower needs to be extended.

The fiber drawing process begins by feeding the glass preform into the drawing furnace. The rate of feeding is usually in the range of 0.1 to 10 mm/min. The furnace is resistively heated and continually purged with argon or nitrogen during the process to prevent the oxidation of the graphite element. The drawing furnace softens the end of the preform (known as 'drop') that is positioned directly below the hot-zone of furnace. The furnace temperature is then increased, and as the preform softens it tapers a neck-down region. The drop falls under gravity and is pulled downwards, by hand, before removing. Then, the fiber is attached to a motorized drum. During this process, pulling speed and preform feed rate are varied and adjusted to keep the fiber diameter constant by monitoring its value by a micrometer. The relative core-cladding dimensions are preserved in this process. In fact, the preform diameter and the fiber diameter are related to the feed speed and pulling speed by:

$$\frac{v_p}{v_f} = \frac{{d_f}^2}{{d_p}^2} \qquad \textbf{(2.5)}$$

where v_p and v_f are respectively the pulling speed and the preform feed, while d_f and d_p are respectively the fiber diameter and the preform diameter.

It is also customary to coat the fiber before winding it up. Typical coating materials are acrylate, silicone and polyimide. The function of the coating is to protect the fiber from abrasion and scratches and preserve its mechanical strength.

2.4 Phosphate Glasses

The main part of this research work was dedicated to the investigation and development of phosphate glasses for fiber laser fabrication. In the first part (Section 2.4.1)of this section a general review of phosphate glasses with an emphasis on the structure is reports, while in the Section 2.4.2a review on the photonic application, in particular fiber laser application, of phosphate glasses is given. At the end (Section 2.5),a state of the art of Yb-doped phosphate glass fiber laser is given.

Research works on phosphate glasses have been stimulated by the wide range of potential and commercial applications of these materials. From the ’50s phosphates glasses have found wide industrial use in the treatment of hard-water, as dispersants in the production of clays and pigments [50]. With the advent of solid state lasers since the '60s, phosphate glasses doped with rare earths, have been widely used as high-power lasers [51]. As bioactive functional materials, phosphate-based glasses find various applications, such as hard and soft tissue engineering and as glasses for controlled release of drugs [52,53]. Polyphosphate glasses have also been found to be responsible for the good anti-wear properties of phosphorus-based engine-oil additives [54]. The chemical stability and low processing temperatures make the amorphous iron-phosphates excellent materials for the storage of radioactive waste [55]. The properties that make phosphate glasses excellent candidates for many and different technological applications are strictly related to their structure at the molecular level.

2.4.1 Structure

In the literature, there are several works regarding the structural study of the phosphates glass, such as those published by Van Wazer [50], Abe [56], Brow[57] and Martin[58]. The basic units that constitute the phosphates glass are the tetrahedra of phosphorus. These tetrahedra are the result of the formation of sp^3 hybrid orbital from the outer electrons $3s^2 3p^3$ of phosphorus. The fifth electron of P is promoted to a 3d orbital that forms a π-bonding molecular orbital with the electrons of the 2p orbital of oxygen. These tetrahedral are connected through bridging oxygen atoms (BO) to give different phosphate anions. The tetrahedral are then classified using the Q_i terminology [57], where 'i' represents the number of tetrahedral linked to the unit (shown schematically in Figure 2.12):

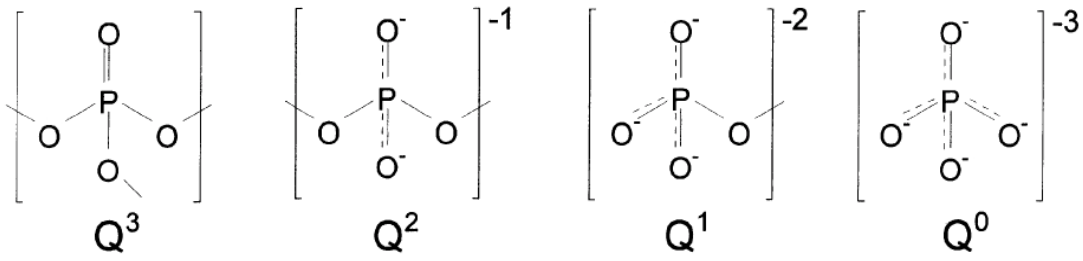

Figure 2.11: Phosphate tetrahedral sites that can exist in phosphate glasses [57]

The system of phosphate glasses can also be described by the oxygen/phosphorus ratio, which determines the number of links between Q-tetrahedral [57]. Considering the $\frac{[O]}{[P]}$ ratio, phosphate glasses can be classified as follows:

- *Ultraphosphate glasses* ($2.5 \leq \frac{[O]}{[P]} \leq 3.0$)
- *Metaphosphate glasses* ($\frac{[O]}{[P]} = 3$)
- *Polyphosphate glasses* ($\frac{[O]}{[P]} > 3$)
- *Pyrophosphates glasses* ($\frac{[O]}{[P]} = 3.5$)
- *Orthophosphates glasses* ($\frac{[O]}{[P]} = 4$)

Phosphate glasses can present a wide variety of structures: they range from Q_3 tetrahedra (P_2O_5 vitreous) systems to meta-phosphates consisting of polymer chains of Q_2 tetrahedra, consisting of glass or pyrophosphate anions (tetrahedral Q_1) or orthophosphate anions (tetrahedral Q_0). The amorphous form of phosphorus pentoxide is called *vitreous* P_2O_5 (*v*-P_2O_5). The $\frac{[O]}{[P]}$ ratio in *v*-P_2O_5 is derived from the stoichiometry of the pure compound and it is equal to 2.5. The basic unit of the structure of the *v*-P_2O_5 is the Q_3 tetrahedron, which has three covalent bonds via bridging oxygen atoms (*BO*) with the neighbours tetrahedral and a terminal shorter bond via non-bridging oxygen atoms (*NBO*). Pure phosphate glasses are not as popular as silicate glasses, because of their poor chemical stability and poor mechanical properties [59-61]. Their application is restricted to specific requirements, e.g. heat-absorbing glasses, HF-resistant glasses, glasses used to measure high-energy radiation. In spite of this, it has been observed that the structural strength and chemical durability of these glasses can be improved by adding appropriate components. Several patents

and papers described the different effect of the different components to the physical and chemical properties of phosphate glass [62-65]. In particular, metal oxides added to v-P_2O_5 can improve physical properties and chemical stability of the system. In more detail, alkali metal oxides R_2O (R = Li, Na, K, Rb and Cs) can be added to the glass to increase the rare earth solubility [66]. When the amount of R_2O is too low, the glass shows poor stability and will devitrify, whereas if the amount of R_2O is too high, the glass will be hygroscopic [67]. Network intermediates R_2O_3 (R = B and/or Al) are also added in phosphate glasses to improve their chemical durability, the mechanical properties and to decrease solubility in water. If the amount of R_2O_3 is too low the glass is water soluble, while if the amount of R_2O_3 is too high, there is an increase in the glass transition temperature and the crystallization temperature [68]. In particular, even a small addition of R_2O_3 can significantly improve the mechanical properties of the phosphate glass. This is due to the particular behavior of R^{3+} ions that can have both tetrahedral and trigonal coordination [68-70]. The presence of alkali-earth oxides MO (M = Mg, Ca, Ba, Sr and Zn) in the glass prevents devitrification and improves the chemical durability [70]. When the amount of MO is too low the glass is hygroscopic and has poor chemical durability and poor optical quality; when the amount of MO is too high, the glass will devitrify [64].

Several analytical techniques, such as NMR [71], Raman and Infrared spectroscopy [72], time-of-flight secondary-ion mass spectroscopy (ToF-SIMS) [73], and XPS [74,75] have been used, over the years, for characterizing the structure of phosphate glasses and then relate the structure of glasses with their chemical, physical and mechanical properties.

2.4.2 Phosphate Laser Glasses

The host glass in which rare-earth ions are incorporated has several important influences on the performance and practical use of an active glass. Factors and properties that must be taken into account in the choice of host glass are: the transparency range, which may exclude certain laser transitions, and the maximum concentration of the dopant ions that can be incorporated without causing clustering of the ions. Furthermore, the host glass influences the optical transitions of the rare earth ions: their wavelengths, emission and absorption cross sections, absorption and emission bandwidth etc [16,76]. In Table 2.2 the typical values of the main characteristics parameters of the common oxide glass-systems used in the near infrared spectral range are reported.

Table 2.2: Comparison of selected properties of common oxide host glasses [5,32,51,77]

Glass property	***Silica***	***Phosphate***	***Tellurite***
Optical Transmission Window [µm]	0.2 ÷ 2.5	0.2 ÷ 4	04 ÷ 5
Phonon Energy [cm^{-1}]	1100	1200	800
Glass Transition Temperature [℃]	1000	500	300
Expansion Coefficient [10^{-6}/℃]	0.5	10	12 ÷ 17
Density [g/cm^3]	2	2.5	5.5
Refractive Index @ 1.55 µm	1.50	1.55	2
RE solubility [ions/cm^3]	10^{19}	10^{21}	10^{21}

Among the glasses for laser applications in the NIR, the interest in phosphate-based laser glasses is increased in the last years. All the leading optical firms involved in the production of laser glass, Schott Glass, Kigre Inc. and Hoya Corp., are currently fabricating active elements from phosphate glasses [78-80]. Phosphate laser glass combines valuable chemical and physical properties that make it a unique and interesting material among conventional oxide glass hosts for rare earth ions.

Many and different studies report the large number of attractive properties that make phosphate glasses suitable as laser media in the near infrared region [81-85]. Phosphate glasses are promising materials for laser application primarily because of their high rare-earth ion solubility, which does not cause quenching of laser emission [85]. In silica, for instance, the rare earth ion concentration can be increased up to ~10^{20} ions/cm^3 before deleterious quenching effect occurs [87,88]. On the other hand, phosphate glasses enable extremely high doping level of rare-earth ions (up to 10^{21} ions/cm^3 [89]) without displaying concentration quenching. This allows appropriately doped phosphate glasses to provide higher optical gain per unit length compared to other glasses. Moreover, the introduction of a quantity of RE ions higher by about 10 times compared to the maximum possible concentration in the silica fiber, allows reducing the length of the active fiber and to increase the threshold of various nonlinear effects in fiber.

In 2000, Jiang et al. demonstrated with a 22 mm long phosphate glass fiber that heavily Er-doped phosphate glasses are excellent materials for compact fiber amplifiers [90]. Moreover, in literature it is reported a cm-long fiber lengths made of highly Er/Yb-doped phosphate glasses that produce up to 2 W of single frequency outputs [91]. Kalrsson et al. described the development of a

highly Er/Yb-doped phosphate glass round plate (Ø 8 x 1 mm) that produced 180 mW of output power in passively Q-switched operation [89].

In addition, phosphate glasses offer a higher photo-darkening threshold than silica, that makes them suitable for the realization of high power, high brilliance laser sources. Lee et al. [92] showed that phosphate fibers can be doped with six times higher Yb^{3+} concentration than Al-doped silica fiber without degradation by photo-darkening effect. Further important feature that makes phosphates glass useful for high power laser applications is their low non-linear refractive index (~$1 \cdot 10^{-13}$ cm^2/V^2), nearly 3 times lower than silica [32]. While the high stimulated emission cross-sections values of the rare-earth ions in phosphate glasses allow a higher pumping efficiency [16].

The phonon energy of phosphate glass is another characteristic that makes them an interesting host for laser applications in the near infrared region. In fact, the value of the phonon energy of phosphate glasses (~1200 cm^{-1}), compared to other host glasses, makes them almost insensitive to up-conversion phenomena [5]. Furthermore, phosphates glasses also have advantages from the point of view of “processability”. In fact, they generally possess lower characteristic temperatures: glass transition temperature (~300-500° C) and melting temperature (~900-1300° C), than most of th e silicate glasses [93,94].

2.5 Yb-doped Phosphate glass fiber laser

State of the Art

After this general overview, the state of the art of phosphate glass fiber laser doped with ytterbium ions is reported below.

The first Yb^{3+}-doped phosphate glass fiber is reported by Kaneda et al. in 2004 [95]. In this study, they have demonstrated a FBR laser at 1.06 μm with >200mW output power. A single-frequency laser with the linewidth of <3 kHz has been achieved from a phosphate glass fiber of only 1.5 cm length.

Lee et al. [96], reported the first cladding-pumped phosphate glass fiber laser doped with 12% by weight of Yb_2O_3. The laser of the study was capable of emitting optical power of about 20W at wavelength of 1.07 μm, in front of a absorbed pump power equal to 60W at a wavelength of 940 nm. The system has an optical efficiency of about 25%. The use of phosphate glass has allowed a heavy concentration of active ions and thereby has allowed reducing the dimension of the active fiber (84.6 cm), without experiencing the typical clustering phenomena of silica fibers. Moreover, in this study two important aspects are highlighted. One relating the remarkable narrow emission peak, since the linewidth at half maximum (FWHM) is equal to 0.25 nm. The other characteristic is the high photodarkening threshold shown by phosphates glasses.

The advantage of reducing the length of the active fiber thanks to the high doping possible for phosphates glasses is clearly shown by an article of 2006 [97]. In fact, Bufetov et al. obtained an output power equal to 250 mW for 670 mW of pump power, with 2.2 cm long phosphate glass fiber. The lasing efficiency with respect the absorbed pump power was 45% at 975 nm.

In literature, a study of ytterbium pulsed systems using phosphate glass fiber is reported by Leigh and co-workers [98]. In 2007, they demonstrated the laser emission in Q-switched mode of a 2 cm long phosphate glass fiber containing about 6% by weight of Yb_2O_3. Q-switching was obtained by using a piezoelectric to press the fiber and modulate the fiber birefringence, so the cavity is switched between high and low loss states. The system was able to work at frequencies of 700kHz with an average power of 31 mW compared with 185 mW of pump provided with a diode laser at a wavelength of 976nm.

In a work of the 2008, Lee et al. reported the performance of a single-mode, single frequency Yb-doped phosphate fiber amplifier [99]. In this work the laser performance of the phosphate fiber compared to [96], were also reported. Thanks to a careful implementation of the set up and the choice of a diode pump laser with a wavelength of emission greater (972 nm, where Yb^{3+} ions absorption is much stronger) than that previous work [96], it was possible to double the slope efficiency of 68-cm long active medium (52.7% of the launched power). Tests carried out to the computer also provide a good performance of the system for even more powers, but one of the main problems is to find a diode pump capable of delivering such radiation intensity.

Lee et al. reported further studies on Yb-doped phosphate fiber amplifier and laser [100]. In 2009, they reported the first watt-level Yb^{3+}-doped phosphate fiber master oscillator power amplifier (MOPA). With approximately 75-cm long double-cladding phosphate fiber, doped with 12% by weight of Yb_2O_3, Lee and co-worker have reached powers of the order of tens of watts (16W), with efficiency greater than 50%. In this work, power scaling to nearly 60 W in a 71-cm long Yb-doped phosphate double-cladding fiber was also demonstrated.

Moreover, the absence of phenomena of photodarkening or non-linear effects allows to simulate operations for powers in the order of hundreds of watts or even kW. Additional measurements of the attenuations (3 dB/m) showed that the losses were related mainly to the absorption process, due to the presence of impurities into the fiber, and less intense by scattering phenomena.

An even greater increase in the concentration of ytterbium ions can lead to a further reduction of the size of the devices. An example is reported by Xu et al. [101], where the lasing effect was obtained with an active region of only 0.8 cm, heavily doped with about 15.2% by weight of Yb_2O_3, which has the highest Yb^{3+}concentration reported in literature.

With the same doping level of Yb_2O_3, Chen et al. [102] demonstrated a fundamentally mode-locked Yb-fiber laser with 3 GHz repetition rate and ~206 fs pulse duration. In this work, using 1 cm heavily Yb-doped phosphate glass fiber as the gain medium and a high-dispersion output coupler for dispersion compensation, the laser self-starts and produces up to 53 mW of average power.

Mo and co-workers recently demonstrated a linearly polarized narrow-linewidth single-frequency fiber laser at 1014 nm [103]. The fiber laser used in this work was based on a 0.5 cm long Yb^{3+}-doped phosphate fiber, with the same doping level of [101]. The output power reported is 164 mW while the linewidth is less than 7 kHz.

Table 2.3: Summary of the state of the art of Yb-doped phosphate fiber lasers (in red the best values for Yb_2O_3 conc., cavity length, output power and slope efficiency are underlined)

	[Yb_2O_3]	cavity length [cm]	output power [W]	slope efficiency %
[95]	-	1.5	0.20	31
[96]	12 wt%	84.6	20	25
[97]	1 x 10^{21} ions cm^{-3}	2.2	0.25	60
[98]	6 wt%	2	0.31	22
[99]	12 wt%	68	25	52
[100]	12 wt%	71.6	57	50
[101]	15.6 wt%	0.8	0.40	72
[102]	15.6 wt%	1	0.05	5
[103]	15.6 wt%	0.5	0.164	22

BIBLIOGRAPHY

1. S.O. Kasap, *Optoelectronics and Photonics*, Prencite-Hall Inc. (2001).
2. J. Downing, *Fiber Optic Communication*, Cengage Learning Press (2004).
3. K. Okamoto, *Fundamental of Optical Wave Guide*, Academic Press Inc.(2006).
4. C.J. Koester and E. Snitzer*,* "Amplification in Fiber Laser"*,* in *Applied Optics,*Vol. 3, Issue 10, pp. 1182-1186 (1964).
5. M.J. Digonett, *Rare-Earth-Doped Fiber Laser and Amplifier*, Marcel Dekker, Inc., (2001).
6. C. Yeh, *Handbook of fiber optics: theory and applications*, Academic Pres Inc. (1990).
7. IPG Photonics Corporation, http://www.ipgphotonics.com
8. N.M. Fried and K.E. Murray, "High-Power Thulium Fiber Laser Ablation of Urinary Tissues at 1.94 μm " in *Journal of Endourology*, 19(1) 25-31(2005).
9. L.M. Veenendaal, A. de Jager, G. Stapper, I.H.M. BorelRinkes, and R. van Hillegersberg, Multiple Fiber Laser-Induced Thermotherapy for Ablation of Large Intrahepatic Tumors in *Photomedicine and Laser Surgery*, 24(1) 3-9 (2006).
10. V.M. Baev, T. Latz and P.E. Toschek, "Laser Intracavity Absorption Spectroscopy",in *Applied Physics*, invited B 69, 171-202 (1999).
11. M. A. Farahani and T. Gogolla "Spontaneous Raman Scattering in Optical Fibers with Modulated Probe Light for Distributed Temperature Raman Remote Sensing" in *Journal of Lightwave Technology*, 17(8), 1379 (1999).
12. R. J. De Young and N. P. Barnes, "Profiling atmospheric water vapor using a fiber laser lidar system" in *Applied Optics*, 49 (4), 562-567 (2010).
13. T. H. Maiman, "Stimulated optical radiation in Ruby," in *Nature,* 187**,** 4736, 493-94, (1960).
14. J.E. Geusic, H.M. Marcos and L.G. Van Uitert, "Laser oscillations in Nd-doped yttrium aluminum, yttrium gallium and gadolinium garnets" in *Applied Physics Letters*4(10), 182-184 (1964).

15. R. Paschotta, J. Nilsson, A. Tropper, and D. Hanna, “Ytterbium-doped fiber amplifiers”, in *Journal of Quantum Electronics, IEEE*, vol. 33, no. 7, pp. 1049–1056, (1997).
16. M.J. Weber, J.E. Lynch, D.H. Blackburn and D. Cronin “Dependence of the stimulated emission cross section of Yb3+ on host glass composition” in *Journal of Quantum Electronics, IEEE* 19(10), 1600-1608 (1983).
17. R. Mears, L. Reekie, S. Poole, and D. Payne, “Neodymium-doped silica single-mode fibre lasers”, in *Electronics letters*, vol. 21, no. 17, pp. 738–740, (1985).
18. E. Snitzer, “Proposed fiber cavities for optical masers,” in *Journal of Applied Physic* 23(1), 36 (1961).
19. R. Mears, L. Reekie, I. Jauncey, and D. Payne, “Low-noise erbium-doped fibre amplifier operating at 1.54 *μ*m”, in *Electronics Letters*, vol. 23, no. 19, pp. 1026–1028, (1987).
20. E. Desurvire, J. Simpson, and P. Becker, “High-gain erbium-doped traveling-wave fiber amplifier”, in *Optics Letters*, vol. 12, no. 11, pp. 888–890,(1987)
21. E. Snitzer and R. Woodcock, “Yb3+ - Er3+ glass laser”, in *Applied Physics Letters*, vol. 6, no. 3, pp. 45–46, (1965).
22. K. Lu and N. Dutta, “Spectroscopic properties of Yb-doped silica glass”, in *Journal of Applied Physics*, vol. 91, no. 2, pp. 576–581, (2002).
23. R. Paschotta, J. Nilsson, P. R. Barber, J. E. Caplen, A. C. Tropper, D. C. Hanna. “Lifetime quenching in Yb-doped fibers”, in *Opt. Commun*. 136:375–378, (1997).
24. V. P. Gapontsev, “*Phosphate Laser Glasses”,* Science, Moscow, 174–386, (1980).
25. E. Snitzer, H. Po, F. Hakimi, R. Tumminelli, and B. McCollum, “Double clad, offset core Nd fiber laser,” in *Optical Fiber Sensors*. Optical Society of America, (1988).
26. H. Po, E. Snitzer, L. Tumminelli, F. Hakimi, N. M. Chu and T. Haw. "Doubly clad high brightness Nd fiber laser pumped by GaAlAs phased array". *Proceedings of the Optical FiberCommunication Conference*. PD7. (1989).
27. V. Dominic, S. MacCormack, R. Waarts, S. Sanders, S. Bicknese, R. Dohle, E. Wolak, P.S. Yeh and E. Zucker, “110W fibre laser” in *Electronics Letters* 35(14), 1158-1160 (1999).

28. Y. Jeong, J.K. Sahu, D.N. Payne and J. Nilsson, “Ytterbium-doped large-core fiber laser with 1.36 kW continuous-wave output power” in Optics Express 12(65), 6088-6092 (2004).
29. H. Po, J.D. Cao, B.M. Laliberte, R.A. Minns, R.F. Robinson, B.H. Rockney, R.R. Tricca and Y.H. Zhang, “High power neodymium-doped single transverse mode fibre laser” in *Electronics Letters*,29(17), 1500 – 1501 (1993).
30. J. Xu, J. Lu, J. Lu and K. Ueda, “Influence of cross-sectional shape on absorption characteristics of double-clad fiber laser” in *Optical Engineering* 42, 2527 (2003).
31. R. Paschotta, *Field Guide to Optical Fiber Technology*, SPIE Field Guides Vol. FG16 (2010).
32. M. Yamane and Y. Asahara, *Glasses for Photonics*, Cambridge University Press, (2004).
33. J. J. Zayhowski, “Q-switched operation of microchip lasers”, in *Optics Letters* 16(8), 575 (1991).
34. J. J. Degnan, “Optimization of passively Q-switched lasers”, in *Journal of Quantum Electron IEEE*31(11), 1890 (1995).
35. T. Hakulinen and O. G. Okhotnikov, “8 ns fiber laser Q switched by the resonant saturable absorber mirror”, in *Optics Letters* 32(18), 2677 (2007).
36. M.C. Gower, “Industrial Application of Laser Micromachining” in *Optics Express*, 7(2), 56-67 (2000).
37. A.J. McGrath, J. Munch, G. Smith and P. Veitch “Injection-seeded, single-frequency, Q-switched erbium:glass laser for remote sensing” in *Applied Optics*, 37(24), (1998).
38. M.E. Fermann and I. Harlt, “Ultra fast laser technology” in Journal of Selected Topics in Quantum Electronics, IEEE 15(1), 191-206 (2009).
39. Y. Yan, E.B. Gamble Jr. and K.A. Nelson, “Impulsive stimulated scattering: General importance in femtosecond laser pulse interactions with matter, and spectroscopic applications” in *Journal Chemical Physic* 83, 5391 (1985).
40. J. Zhang, J. Y. Huang, H. Wang, K. S. Wong and G. K. Wong “Second-harmonic generation from regeneratively amplified femtosecond laser pulses in BBO and LBO crystals” in *Journal of Optical Society American B* 15(1) (1998).
41. X. Liu, D. Du and G. Mourou “Laser ablation and micromachining with ultrashort laser pulses ” in *Journal of Quantum Electronics*, IEEE, 33(10), 1706 – 1716, (1997)

42. Fibercore Ltd., http://www.fibercore.com/
43. D.B. Keck, P.C. Shultz and F. Zimar: US Patent 3 737 292, (1973).
44. J. B. MacChesney, P. B. O'Conner and H. M. Presby: *Proc. IEEE* 62 1278 (1974).
45. T. Izawa, T. Miyashita and F. Hanawa: *Proc. Int. Conf. Integrated Optics and Optical Fiber Communication* 375. (1977).
46. E.T.Y. Lee, E.R.M. Taylor, "Two-die assembly for the extrusion of glasses with dissimilar thermal properties for fibre optic preforms", in *Journal of Materials Processing Technology*, 184, 325 (2007)
47. S. Mitachi, Y. Ohishi, T. Miyashita, "A fluoride glass optical fiber operating in the mid-infrared wavelength range", in *Journal of Lightwave Technology*, LT-1 67 (1983).
48. N. Peyhgambarian and S. Jiang, US Patent 6 611 372 B1 (2003).
49. D.C. Tran, C.F. Fischer and G.H. Sigel "Fluoride glass preforms prepared by a rotational casting process" in *Electronics Letters* 18 657–658 (1982).
50. J.R. Van Wazer, Phosphorus and its Compounds, vol. 1, Interscience Press (1958).
51. J.H Campbell, T.I Suratwala "Nd-doped phosphate glasses for high-energy/high-peak-power lasers" in *Journal of Non-Crystalline Solids*, 263–264, 318–341 (2000).
52. E. A. Abou Neel, D. M. Pickup, S. P. Valappil, R. J. Newport, and J. C. Knowles, "Bioactive functional materials: a perspective on phosphate-based glasses", in Journal of Materials Chemistry, 19, 690-701 (2009).
53. D. Muresan, M. Dragan, Bularda, C. Popa, L. Baia, and S. Simon: "Structural and biological investigation of phosphate glasses with silver", in *Biophysics, Environmental Physics*, 232-237 (2004).
54. J.M. Martin, "Antiwear mechanisms of zinc dithiophosphate: a chemical hardness approach" in *Tribology Letters*, 6, 1-8, (1999).
55. K, Xu, P. Hrma, W. Um, J. Heo, "Iron phosphate glass for immobilization of ^{99}Tc", in *Journal of Nuclear Materials*, 441, 262-266, (2013).
56. Y. Abe, *Topics in Phosphorus Chemistry*, vol. 11, Wiley, New York, M. Grayson, E.J. Griffith (Ed.), (1983)
57. R. K. Brow, "Review: the structure of simple phosphate glasses" in *Journal of Non-Crystalline Solids*, 263&264, 1-28, (2000).

58. S. W. Martin, “Ionic Conduction in Phosphate Glasses”, in *Journal of the American Ceramic Society* 74(8), 1767–1784, (1991).
59. L.G. Baikova, V.P. Pukh, Y. K. Fedorov, A.B. Sinani, L.V. Tikhonova, and M.F. Kireenko, “Mechanical properties of phosphate glasses as a function of the total bonding energy per unit volume of glass” in *Glass Physic Chemistry*, 34, 126-131 (2008).
60. C. R. Kurkjian, “Mechanical properties of phosphate glasses” Journal of Non-Crystalline Solids 263-264, 207-212 (2000).
61. M. Karabulut, E. Melnik, R. Stefan, G. K. Marasinghe, C. S. Ray, C. R. Kurkjian, and D. E. Day, “Mechanical and structural properties of phosphate glasses” in *Journal of Non-Crystalline Solids* 288, 8-17 (2001).
62. J.D. Myers and C.S. Vollers, US Patent 4 075 120 (1978).
63. J. Hayden, US Patent 5 334 559 (1994).
64. J.D. Myers and C.S. Vollers, US Patent 4 248 732 (1981).
65. R.K Brow, C.A Click, T.M Alam, “Modifier coordination and phosphate glass networks” in *Physics of Non-Crystalline Solids* 227(1-6), 9-16, (2000).
66. K. Seneschal, F. Smektala, B. Bureaua,, M. Le Flocha, S. Jiang, T. Luo, J. Lucas and N. Peyghambarian “Properties and structure of high erbium doped phosphate glass for short optical fibers amplifiers” in *Materials Research Bulletin* 40, 1433–1442, (2005).
67. N. El-Shafi, S. Ibrahim, A. Ali, “Chemical durability of some P2O5-PbO-Al2O3-R2O glasses”, in *Physics and Chemistry of Glasses -EUROPEAN JOURNAL OF GLASS SCIENCE AND TECHNOLOGY PART B*50(1), 45-51,(2009).
68. T. Harada, H. In, H. Takebe and K. Morinaga, “Effect of B_2O_3addition on the thermal stability of barium phosphate glasses for optical fiber devices” in *Journal of American Ceramic Society* 87(3), 408-411 (2004).
69. R.K Brow “Nature of Alumina in Phosphate Glass: I, Properties of Sodium Aluminophosphate Glass” in *Journal of the American Ceramic Society* 76(4), 913-918, (1993).
70. P.A. Bingham, R.J. Hand, O.M. Hannant, S.D. Forder, S.H. Kilcoyne “Effects of modifier additions on the thermal properties, chemical durability, oxidation state and structure of iron phosphate glasses” in *Journal of Non-Crystalline Solids*, 355(28–30), 1526-1538 (2009).

71. J.W. Wiench, B. Tischendorf, J.U. Otaigbe and M.Pruski, “Structure of zinc polyphosphate glasses studied by two-dimensional solid and liquid state NMR”, in *Journal of Molecular Structure*, 2002. 602-603: p. 145-157.
72. K. Meyer, “Characterization of the structure of binary zinc ultraphosphate glasses by infrared and Raman spectroscopy” in *Journal of Non-Crystalline Solids*,. 209(3): 227-239 (1997),
73. H.B. Lu, C.T. Campbell, D.J. Graham and B.D.Ratner, “Surface Characterization of Hydroxyapatite and Related Calcium Phosphates by XPS and TOF-SIMS” in *Analytical Chemistry*, 72(13): 2886-2894. (2000).
74. R.K. Brow, “An XPS study of oxygen bonding in zinc phosphate and zinc borophosphate glasses” in *Journal of Non-Crystalline Solids*, 194(3), 267- 273 (1996).
75. R.K. Brow, C.M. Arens, X. Yu and E. Day, “An XPS Study of Iron Phosphate Glasses” in *Physics and Chemistry of Glasses*, 35(3), 132-136, (1994).
76. M.J. Weber, “Science and Technology of Laser Glass”, in *Journal of Non-Crystalline Solids*, 132, 208-222 (1990).
77. J.S. Wang, E.M. Vogel and E. Snitzer, “Tellurite glass: a new candidate for fiber device”, in Optical Materials, 3, 187-203, (1994).
78. Schott Glass, http://www.schott.com/
79. Kigre Inc., http://www.kigre.com/
80. Hoya Corp., http://www.hoya.co.jp/
81. K. Seneschal, F. Smektala, S. Jiang, T. Luo, B. Bureau, J. Lucas, N. Peyghambarian “Alkaline-free phosphate glasses for ultra compact optical fiber amplifiers at 1.5 μm” in *Journal of Non-Crystalline Solids*324 (1–2), 179-186 (2003).
82. D. L. Veasey, D. S. Funk, P. M. Peters, N. A. Sanford, G. E. Obarski, N. Fontaine, M. Young, A. P. Paskin, W. Liu, S. N. Houde-Walter, J. S. Hayden, “Yb/Er-codoped and Yb-doped waveguide lasers in phosphate glass” in *Journal of Non-Crystalline Solids* 263&264, 369-388, (2000).
83. J.D. Myers and M.J. Myers, US Patent 6 911 160 (2005).
84. C. Florea and K. A. Winick, “Ytterbium-Doped Glass Waveguide Laser Fabricated by Ion Exchange” in *Journal of Lightwave Technology*, 17(9), (1999).

85. L. I. Avakyants, V. I. Molev, A. E. Pozdnyakov and V. F. Surkova, “A new phosphate laser glass” in *Journal of Optical Technology*”, 71(12), 828-829, (2004).
86. V.P. Gapontsev, S.M. Matitsin, A.A. Isineev, V.B. Kravchenko, “Erbium glass lasers and their applications” in *Optics & Laser Technology* 14(4), 189–196 (1982).
87. R. S. Quimby,W. J. MiniscalcoandB. Thompson, “Clustering in erbium-doped silica glass fibers analyzed using 980 nm excitedstate absorption” in *Journal of Applied Physics*, 76(8),4472-4478, (1994).
88. F. Auzel P. Goldner “Towards rare-earth clustering control in doped glasses” in *Optical Materials* 16, (1–2), 93–103 (2001).
89. G. Karlsson, F. Laurel, J. Tellefsen, B. Denker, B. Galagan, V. Osiko and S. Sverchkov, “Development and characterization of Yb-Er laser glass for high average power laser diode pumping” in *Applied Physics B*, 75, 41-46, (2002)
90. S. Jiang, T. Luo, B. Hwang, F. Smekatala, K. Seneschal, J. Lucas, N. Peyghambarian “Er3+.-doped phosphate glasses for fiber amplifiers with high gain per unit length” in *Journal of Non-Crystalline Solids* 263&264 364-368 (2000).
91. C. Spiegelberg, J. Geng, Y. Hu, Y. Kaneda, S. Jiang, and N. Peyghambarian, “Low-Noise Narrow-Linewidth Fiber Laser at 1550 nm”, in *Journal of Lightwave Technology*, 22(1), 57-62, (2004)
92. Y.W. Lee, S. Sinha, M.J.F. Digonnet, R.L. Byer and S. Jiang “Measurement of high photodarkening resistance in heavily Yb3+-doped phosphate fibres” in *Electronics Letters*, 44(1), (2008).
93. C.Weng, J. Chen, P. Shih “Effect of dehydroxylation on the structure and properties of $ZnCl_2$–ZnO–P_2O_5 glasses” in *Materials Chemistry and Physics*115, 2–3, 628–631 (2009).
94. S. Rani, S. Sanghi, A. Agarwal, N. Ahlawat, “Influence of Bi_2O_3 on optical properties and structure of bismuth lithium phosphate glasses”,in *Journal of Alloys and Compounds,*477, 504, (2009).
95. Y. Kaneda, C. Spiegelberg, J. Geng, Y. Hu, T. Luo, J. Wang and S. Jiang, “200-mW, narrow-linewidth 1064.2-nm Yb-doped fiber laser”in*Proceeding of IEEE Conference on Lasers and Electro-Optics IEEE* paper CThO3, (2004)

96. Y. W. Lee, S. Sinha, M. J. F. Digonnet, and R. L. Byer and S. Jiang,“20W single-mode Yb3+-doped phosphate fiber laser” in *Optics Letters*, 31(22), 3255-3257, (2006).
97. LA. Bufetov, S.L. Semenov, A.F. Kosolapov, M.A. Mel'kumov, V.V. Dudin, B.I. Galagan, B.I. Denker, V.V. Osiko, S.E. Sverchkov, E.M. DianovI “Ytterbium fiber laser with heavily Yb3+-doped glass fiber core”, in *Quantum Electronics*, 36(3), 189-191, (2006).
98. M. Leigh, W. Shi, J. Zong, J. Wang, S. Jiang and N. Peyghambarian, “Compact, single-frequency all-fiber Q-switched laser at 1 μm” in *Optics Letters*, 32(8), 897-899, (2007).
99. Y. W. Lee, S. Sinha, M. J. F. Digonnet, R. L. Byer and S. Jiang “10-watt, single-mode, single-frequency, 1.03 μm Yb3+-doped phosphate fiber amplifier” in *Proceeding IEEE Optical Society of America*, 978-1-55752-859-9, (2008).
100. Y. W. Lee, M. J. F. Digonnet, S. Sinha, K. E. Urbanek, R. L. Byer and S. JiangY, “High-power Yb3+-doped phosphate fiber amplifier”, in *Journal of Selected Topics in Quantum Electronics IEEE*, 15(1), 93-102 (2009).
101. S. Xu, Z. Yang, W. Zhang, X. Wei, Q. Qian, D. Chen, Q. Zhang, S. Shen, M. Peng, and J. Qiuet “400 mWultrashort cavity low-noise single-frequency Yb3+-doped phosphate fiber laser” in *Optics Letters*, 36(18), 3780-3710 (2011).
102. H. Chen, G. Chang, S. Xu, Z. Yang and F.X. Kärtner, “3 GHz, fundamentally mode-locked, femtosecond Yb-fiber laser” in *Optics Express*, 37(17), 3522-3524 (2012).
103. S. Mo, S. Xu, X. Huang, W. Zhang, Z. Feng, D. Chen, T. Yang and Z. Yang, “A 1014 nm linearly polarized low noise narrowlinewidth single-frequency fiber laser” in *Optics Express*, 21(10), (2013).

Chapter 3

Experimental Work

3.1 Bulk Glass

One of the main goals of this research work was to define and optimize new phosphate glass compositions to be used in the manufacture of optical fibers and fiber lasers. The aim was to obtain optical glasses with high purity and high homogeneity to allow the propagation of light beam with minimum optical losses. Moreover, these glasses had to show great stability against crystallization (T_x – T_g) to be drawn into optical fibers. In the following sections, the different processes and measurements used to prepare and characterize the glasses object of this work are presented and described.

3.1.1 Sample preparation

In phosphate glasses, the glass-former (P_2O_5) is very reactive and difficult to form a glass without the addiction of other components to the melts. If the amount of P_2O_5 is too high *(>65mol%*) there is a tendency toward crystallization and poor chemical durability. On the other hand, if the amount of P_2O_5 is too low *(<40%mol*), devitrification occurs thereby preventing formation of glass. Nevertheless, many constituents can be added to the composition to improve physical properties and chemical stability of the phosphate glass [1-4].

During this work, multi-components phosphate based glasses were designed by selecting the type and the amount of each glass constituent. Specifically, alkali metal oxides (R_2O, where R is Li) were added to the glass to lower process temperature; while alkali-earth oxides (MO, where M is Mg and/or Ba) were added to the glass to prevent devitrification and to improve the chemical durability; network intermediates (X_2O_3, where X is Al, B, La) were also added to improve the chemical durability and mechanical properties, and to decrease the solubility in water. Several phosphate glass compositions were prepared through melt-quenching technique and characterized. In Table 3.1 the different sets of phosphate glass-compositions fabricated during this research work are shown. For each glass sample, the amounts of raw materials required have been calculated as the mol% of each component of the glass and weighed to produce the reaction mixture.

Table 3.1: Sets of phosphate glass compositions studied; [a] Yb_2O_3 added as wt% to the cast glass

	Glass	Composition (mol%)								
		P_2O_5	Al_2O_3	Li_2O	BaO	B_2O_3	La_2O_3	PbO	MgO	Yb_2O_3
Method 1	PAL 01	65	3	17	5	4	6	-	-	-
	PAL 02	65	3	18	4	4	6	-	-	-
	PAL 03	65	3	19	3	4	6	-	-	-
	PAL 04	65	3	20	2	4	6	-	-	-
Method 2	PAL 05	65	3	9	5	4	7	7	-	-
	PAL 06	65	3	14	4	4	7	5	-	-
	PAL 07	65	8	20	3	4	-	-	3	-
	Yb 01	65	3	9	5	4	3.5	7	-	3.5
	PAL 08	65	3	16	2	4	7	3	-	-
Method 3	Yb 02	65	3	9	5	4	5.9	7		1.1
	PAL 09	65	3	14	4	4	7	5	-	-
	PAL 10	65	8	20	3	4	-	-	3	-
Method 4	Yb03	65	3	9	5	4	7	7	-	(1.1)[a]
	PAL 11	65	3	9	5	4	7	7	-	-
	PAL 12	65	8	20	3	4	-	-	3	-

Various tests were performed and glass candidates for fiber drawing process were selected upon their thermal and optical properties. Different optical fibers were drawn from the different sets of glasses. Throughout the course of this research work, it was still necessary to modify or adjust both the compositions and the methods of glass fabrication, in order to optimize the quality of the fibers. Overall four different methods were used in this research

work for glasses manufacturing are shown below:

- **Method 1**

The first set (PAL01, 02, 03 and 04 compositions) of multi-components phosphate based glass was prepared by mixing the following high purity (*>99.99%*) chemicals in powder form: P_2O_5, Al_2O_3, Li_2CO_3, H_3BO_3, $BaCO_3$, La_2O_3. The chemicals were weighted within a glove box under dried air atmosphere and were fused twice in order to improve the homogeneity of the glass: the melting was carried out in alumina crucible. To reduce the contamination of atmospheric water, the whole process was carried out by blowing 3 l/min of a mixture of dry N_2/O_2into the furnace. As preliminary tests, small batches (*30g*) were first pre-treated at 300℃ for 1h in a chamber furnace (*Carbolite RHF 1800, Hope Valley, UK*) and then melted for 2h in covered alumina crucible at 1500℃ - 1600℃, depending on the composition. The molten glass was cast in a pre-heated brass plate to prevent cracks on the produced glass. Then the formed glass was annealed at 10℃ below the glass transition tempera ture for 5 h to remove thermal stress. The glass sample was then cooled down slowly to room temperature.

- **Method 2**

For the second set (PAL05, 06, 07, 08 and Yb01 compositions) of multi-component phosphate glasses the following chemicals in powder form and high purity (*>99.99%*) were weighted and mixed within a glovebox under dried air atmosphere: P_2O_5, Al_2O_3, Li_2CO_3, H_3BO_3, $BaCO_3$, La_2O_3, *PbO, MgO and* Yb_2O_3. Also this set of glasses underwent a melting process in alumina crucible. To

minimize water content, the process was carried out by blowing 3 l/min of a mixture of N_2/O_2into the furnace. Batches of 30gwere melted in 'bottom loading' furnace (*Proba*) in covered alumina crucible at 1400℃ for 1h. The molten glass was cast in a pre-heated brass plate and then annealed at 10℃ below the glass transition temperature for 5 h. The glass sample was then cooled down slowly to room temperature.

- **Method 3**

A third set of glasses (Yb02, PAL09 and PAL10 compositions) was prepared by mixing the following high purity (>99.99%) chemicals in powder form: $NH_4H_2PO_4$, Al_2O_3, Li_2CO_3, H_3BO_3, $BaCO_3$, La_2O_3, PbO, MgO and Yb_2O_3.In this set of glasses, the glass-former phosphorus pentoxide (P_2O_5) was replaced by ammonium di-hydrogen phosphate ($NH_4H_2PO_4$). During heating, the reagent $NH_4H_2PO_4$ is thermally decomposed in phosphorus pentoxide, water and ammonia. For this reason the precursor ($NH_4H_2PO_4$) alone was pre-heated at 250℃ for 2h while blowing 5 l/min of N_2 into the furnace. Then the remaining chemicals, weighted within a glove box under dried air atmosphere, were add to the batch. Batches of 40g were melted in 'bottom loading' furnace (*Proba*) in covered alumina crucible at 1400℃ for 1h. To reduc e the contamination of water present in air, all the process was carried out by blowing 3 l/min of a mixture of dry N_2/O_2 into the furnace. The molten glass was cast in a pre-heated brass plate and then annealed at 10 ℃ below the glass transition temperature for 5 h. The glass sample was then cooled down slowly to room temperature.

- **Method 4**

A single batch for both core and first cladding glasses were prepared.The following chemicals in powder form of high purity (*>99.99%*) were weighted and mixed within a glove box under dried air atmosphere: P_2O_5, Al_2O_3, Li_2CO_3, H_3BO_3, $BaCO_3$, La_2O_3, *PbO, MgO and* Yb_2O_3. The chemicals of the cladding glass composition were weighed within a glove box in an amount double (*80 g*) than the third fabrication method. This batch was melted in 'bottom loading' furnace (*Proba*) in covered alumina crucible at 1400 ℃ for 30 min. The glass mass obtained was then divided into two parts of equal mass: one for the core glass, the other for the cladding glass. The desired amount of Yb_2O_3 was added to the grinded glass part destined to the core.The core glass was melted again at 1350℃ in order to homogenize the glass and to inco rporate the ytterbium oxide. Also for this method, to reduce the contamination of water present in air, the process was carried out by blowing 3 l/min of a mixture of N_2/O_2 into the furnace. For each casting, the molten glass was cast in a pre-heated brass plate. Then the formed glass was annealed at 10℃ below the gla ss transition temperature for 5 h to remove any thermal stress into a square brass mould. The glass sample was then cooled down slowly to room temperature.

3.2 Glass characterization

3.2.1 Differential Thermal Analysis (DTA)and Differential Scanning Calorimetry (DSC)

Differential Thermal Analysis (DTA) and Differential Scanning Calorimetry (DSC) techniques have been used in this study to determine the characteristic temperatures (glass transition temperature, T_g, onset of crystallization, T_x) of the prepared samples. From these information the T_x–T_g gap can be calculated, which is a estimate of glass stability, and an important consideration for fibre-drawing process, since the width of this temperature range is proportional to the stability of the glass against crystallisation.

In our study, the differential thermal analysis was performed using a commercial DTA 404PC apparatus from Netzsch GmbH. The test provides two cells placed in a heating chamber. In a cell there is the sample to be tested, while in the other there is the reference (Al_2O_3). During DTA test, any difference in temperature between the sample and a reference is recorded. About 35 mg of finely ground glass samples was used for each measurement. The analyses were performed up to 1400℃ with a heating rate of 10℃/min. In Figure 3.1 an example of a thermogram obtained for a glass is shown. The glass transition temperature (T_g) and the crystallization temperature (T_x) of the prepared samples were measured by differential thermal analysis (*DTA*) calorimeter.

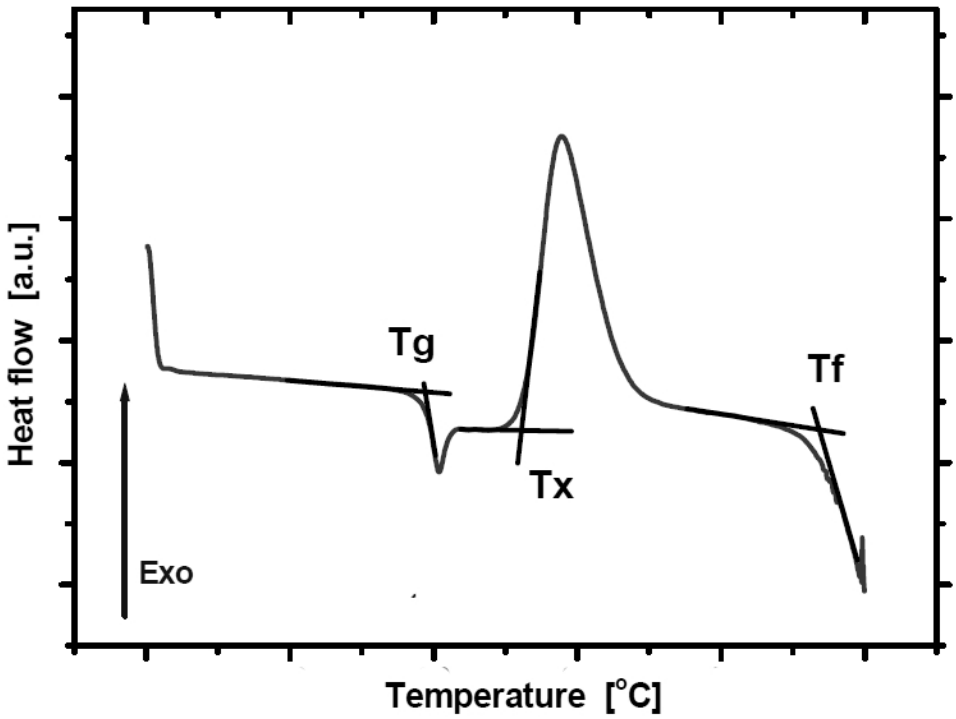

Figure 3.1: DTA thermogram: glass transition temperature, T_g; crystallization temperature, T_x; fusion temperature, T_f

The glass transition temperature (T_g) and the crystallization temperature (T_x) of the prepared samples were measured as follow. The glass transition is an endothermic process. The glass transition temperature wasextrapolated fromthe inflection point of the endothermic peak by taking the first derivative of the curve. Crystallizationis an exothermic process and crystallization temperature was taken at the inflection point of the exothermic peak (by taking the first derivate of the curve) as illustrated in Figure3.1. The accuracy of the measurements was estimated to be ± 3℃.

The DSC equipment used in this study was a DSC7 Perkin Elmer calorimeter with a water recirculating chiller and an argon gas flow. The

instrument has separate furnaces for sample and reference, each with a thermocouple Glass samples of around 20 mg were sealed in aluminum pans using a pan press. As reference an empty aluminum crucible was used. The analyses were performed up to 600℃ with a heating rate of 10℃/min. For each DSC experiment, a baseline run taken with the same ramp program using empty pans was subtracted. From the DSC thermogram, the characteristic temperatures of the prepared samples were measured in the same way as in the case of DTA thermogram.

3.2.2 Density

Density is defined as the mass of the substance per unit of volume [g/cm^3]. The density of the prepared glasses was measured at room temperature by the Archimedes' method using distilled water as immersion liquid; three independent measurements were carried out for each sample.

In the Archimede's method the sample is first weighted in air and then when immersed in distilled water. From these to weightings, density is calculated as follow:

$$W_{liq} = W_{air} - F_{Arc} \qquad (3.1)$$

where W_{liq} is the weight of the sample in distilled water; W_{air} is the weight of the sample in air and F_{Arc} is the Archimedes' force. The Equation 3.1 can be re-written as follow:

$$W_{liq} * g = W_{air} * g - V * \rho_0 * g \qquad (3.2)$$

with $V = W_{air} / \rho_{sample}$

Hence:

$$\rho_{sample} = \frac{W_{air}}{W_{air} - W_{liq}} \qquad (3.3)$$

The accuracy of the measurements was estimated to be ± 0.01 g/cm^3.

3.2.3 Refractive Index

While for the thermal analysis it was sufficient to mill a few milligrams of glass from the sample, for the optical characterizations, especially for the refractive index measurements, it was necessary to polish the samples to obtain an excellent surface quality. Once extracted from the mould, each bulk glass sample was cut into one or more square samples (20mmx20mm) through precision saw with circular diamond coated blade. Each specimen was lapped and polished with a Logitech PM5 machine. The lapping was carried out on a cast iron rotating plate with a suspension of 9 µm size alumina powder in water or ethanol (*99.99%*). Then, polishing using a polyurethane plate with 1 µm size diamond paste in water followed.

The refractive index measurements were carried out using the prism coupling method, with the instrument Metricon2010/M capable of measuring the index at five different wavelengths: 633, 825, 1061, 1312 and 1533nm [5].

Refractive indices are determined from the measurement of the angle incident to the prism at which total reflection on the prism base breaks (Figure 3.3).

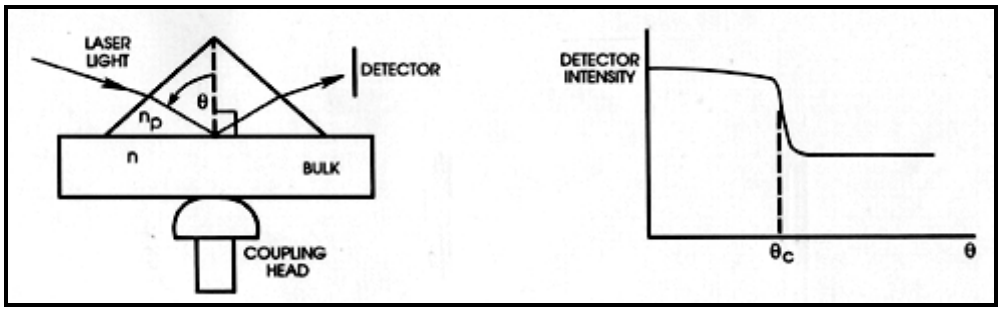

Figure 3.3:Schematic illustration of prism coupling method: measurement and calculation of the refractive index [5]

Laser light directed onto the base of the prism will be totally reflected at the prism base until the angle of incidence Θ becomes less than the critical angle Θ_c:

$$\theta_c = \arcsin\left(n/n_p\right) \qquad (3.4)$$

where n is the refractive index of the sample and n_p is the refractive index of the prism. Θ_c is easily measured since the detector intensity drops abruptly as Θ drops below the critical angle (see Figure3.3) and light starts to leak into the bulk material. Since n_p is known, n (the refractive index of the sample) can then be determined from Equation 3.4.The accuracy of the measurements was estimated to be $\pm 10^{-3}$.

3.2.4 UV-Vis spectroscopy

In this research work, the UV-Vis-NIR absorption spectra of the samples were measured with a dual beam Varian Cary 5000 UV-Vis-NIR spectrophotometer at different scan rates in the 200- 3000 nm region. In the experimental set-up, the beam was focused onto the sample, with the light incident on the sample at normal angle. The sample was optically polished and thoroughly cleaned before any measurement (see Section 3.2.3). In this arrangement, the amount of light transmitted is compared with the source beam and the amount of light absorbed is calculated as a function of the wavelength of the beam to obtain the spectra. In the case of rare-earth ion doped glasses, the spectra were used to calculate the absorption cross-section (σ_{ass}) of the Yb^{3+} ions. The absorption cross-section is defined as follow:

$$\sigma_{ass} = \frac{\alpha(\lambda)}{N} \qquad (3.5)$$

where ***α(λ)*** is the absorption coefficient measured at the wavelength *λ*; ***N*** is the ions density of the active ion expressed as [ions/cm^3]. *α(λ)* is obtained from the absorbance *A* and transmittance *T*:

$$A = ln\frac{I}{I_0} \qquad (3.6)$$

$$T = \frac{I}{I_0} = e^{(-\alpha L)} \qquad (3.7)$$

$$\alpha(\lambda) = \frac{2.303 \cdot A}{L} \qquad (3.8)$$

where *L* is the thickness of the sample.

The absorption coefficient is quickly obtained with appropriate substitutions:

$$\sigma_{ass} = \frac{2.303 \cdot A}{L \cdot N} \qquad (3.9)$$

The thickness *L* of the samples was measured with caliber, while the ions density *N* was calculated by:

$$N = \frac{wt\%_{Yb_2O_3}}{MW_{Yb_2O_3}} \cdot 2 \cdot N_A \cdot \rho \qquad (3.10)$$

where $wt\%_{Yb2O3}$ is the weight percentage of Yb_2O_3; MW_{Yb2O3} is the molecular weight of Yb_2O_3; N_A is the Avogadro's number; ρ is the density of the glass expressed as [g/cm^3].

3.2.5 Life-Time measurements

The values of lifetime are calculated analytically from measurements of fluorescence. For these measurements a diode laser with an emission at a wavelength centered at 915 nm has been used as a pump (OclaroBMU8-915-01-R). The output power of the laser was modulated with an external generator of square wave, working in synchrony with the laser, generating pulses, and with the oscilloscope, providing the reference signal. The emission intensity of the sample was then recorded as a function of time. The detector used was Thorlabs

PDA 10CS-EC. Since the detector operates in a wide range of wavelengths, in which also falls to pump, was preceded by a filter (ThorlabsFEL950) to eliminate the wavelengths below 950 nm. The experimental data were fitted by an exponential fit: exp(t/τ).

3.3 Fiber fabrication

After the complete characterization of the glass samples, specific glass compositions were selected to fabricate the optical fiber from performs drawing. The phosphate glass performs were fabricated by rod-in-tube method. In the following section, an overview of the preforms and fiber fabrication processes involved in this work is described.

3.3.1 Preform Fabrication Process and Fiber Drawing Process

A key fabrication step to assure a good quality of the resulting fiber is preform fabrication. The phosphate glass preforms used for the following fiber drawing of this study were produced using the rod-in-tube technique. In particular, the rotational casting process was used in this study to fabricate the cladding tubes of phosphate glass.

Two glass samples previously molten inside alumina crucibles were in general required to prepare one preform tube. This second melting step was carried out in a platinum crucible, which could be easily cleaned and re-used.

The rod-in-tube technique is based on individual preparation of core and cladding compositions. This technique is schematically shown in Figure 3.5.

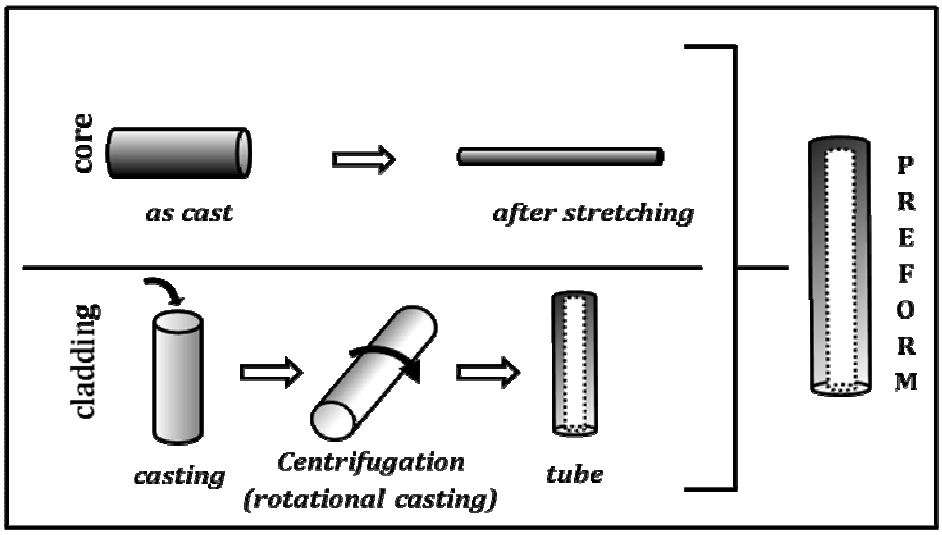

Figure 3.5: Scheme of the rod-in-tube preform fabrication process

Core rod

The first step of preform fabrication was to manufacture the core glass rod. The glass selected for the core composition was weighed (*60g*) melted and then poured into a cylindrical pre-heated brass mould with 11 cm of internal diameter. The mould with the core rod was placed into an annealing furnace for 48 h. Casting temperature, mould pre-heating temperature and glass annealing temperature were evaluated and optimized for the different core glass compositions, in order to obtain rods free of cracks and bubbles. After the annealing process, the core rod was carefully polished with SiC papers (*Presi, France*) of different grits: 100,120, 320, 600, 800, 1000, 1200, 2400 mesh. The polishing process was then completed with diamond paste of 1 µm in order to obtain excellent surface quality.Ethanol (*99.99%*) was used as lubricant coolant

during the polishing process. In Figure 3.4 an example of a core rod after the polishing process is shown.

Figure 3.5: Photograph of a core rod after polishing

Cladding tubes

The cladding tubes used in this work were produced by rotational casting technique. In-house built-up rotational casting apparatus was used to fabricate the cladding tubes. A part of this research work has been devoted to the design and the optimization of a new rotational casting equipment (Figure 3.6 and 3.7). Design of the individual parts were done using Autocad 3D.

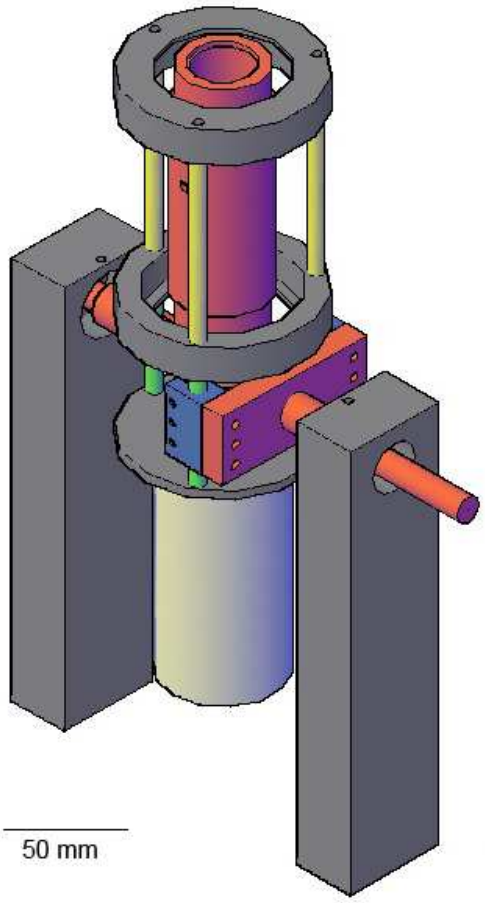

Figure 3.6: Scheme of the rotational casting equipment designed for the cladding tubes fabrication

Figure 3.7: Rotational casting equipment used for the cladding tubes fabrication

The selected cladding glass composition (*60g*) was melted and then cast into a cylindrical mould. The equipment was then quickly rotated horizontally and the mould was spun for few second. Finally, the mould with the cladding tube was placed into the annealing furnace for 48 h. After the annealing process, as for the core rods, the cladding tubes were carefully polished with SiC papers of different grits from 100 down to 4000 mesh, in order to obtain optical quality surface finish. In Figure 3.8 is shown an example of a cladding tube obtained by rotational casting.

Figure 3.8: Photograph of a cladding tube after polishing

The parameters of the rotational casting process (rotation speed and time, casting temperature and mould temperature) were evaluated and optimized through a series of repeated experiments for the different cladding glass compositions in order to obtain cladding tubes with controlled and reproducible internal diameter.

For the single cladding fibers, the core rod was then stretched in the drawing tower to fit the internal diameter of the cladding tube. An additional stage was required for the fabrication of the preform for double-cladding fibers. After introducing the stretched core rod within the first cladding tube, the core/first clad structure was then stretched in the drawing tower to fit the second cladding tube.

In the fiber drawing process, the preforms were heated in a in-house developed drawing tower through a vertical cylindrical induction furnace using a graphite susceptor (see Figure 3.9).

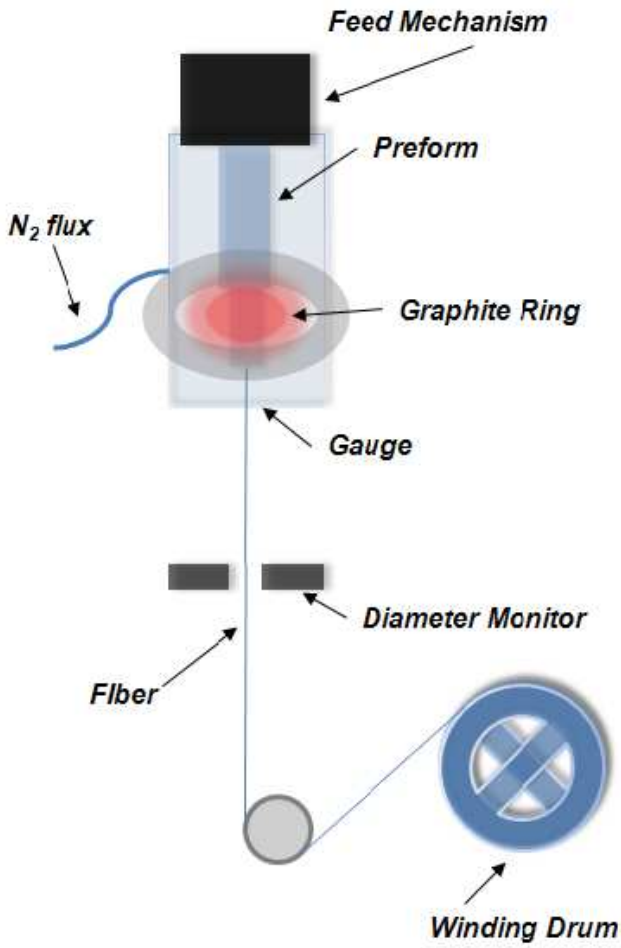

Figure 3.9: Scheme of the drawing tower used for the fiber fabrication process

The furnace is heated by induction and is continually purged with nitrogen during operation to prevent the graphite elements from oxidizing. Glass preforms were lowered into the hot-zone of the furnace and held there until the glass softened and necked down. The dropped glass fell under gravity and the fiber was pulled manually onto the drum and attached with tape. The preform was then fed, and the drum rotated until most of the preform had been used. The preform feed rate and the drum speed were tuned in order to match the targeted fiber diameter. The fiber diameter was continuously monitored during drawing the process. The morphology of the fiber was then measured by using a Nikon

Eclipse 50i optical microscope in order to assess the correct dimensions, geometry and relative positions of core and claddings together with the quality of the core/clad and $1^{st}/2^{nd}$ clad interfaces. The near field image of the fiber output beam was collected on a Grundig electronic SN76 IR videocamera.

3.4 Fiber Performances

In the following section an overview of the fiber characterization and laser demonstration achieved in this work is given. All experimental details and results are given and discussed in Chapter 4.

3.4.1 Optical loss measurement – Cut-Back method

Fiber optical loss measurements were performed using cut-back method as shown in Figure 3.10.

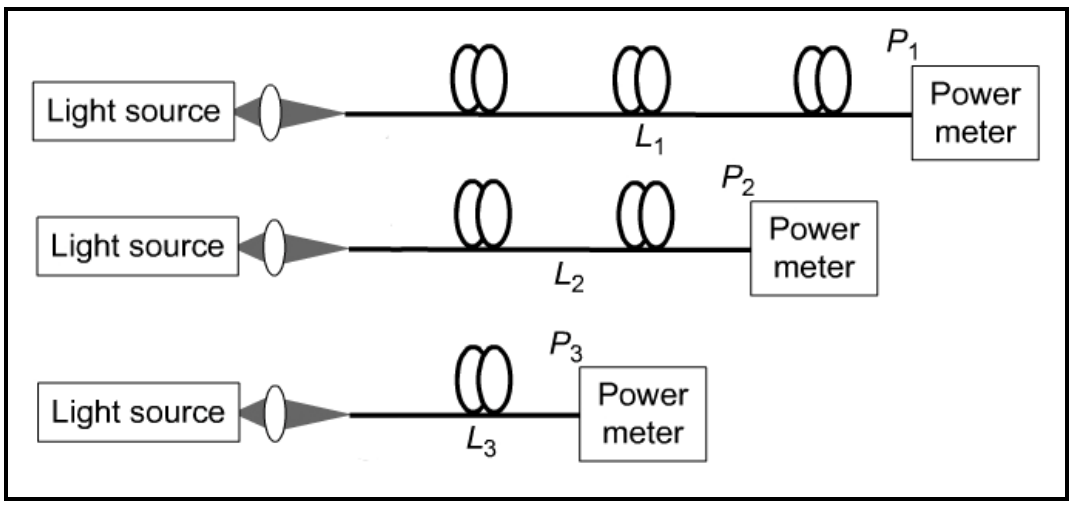

Figure 3.10: Set-up used for the attenuation losses measurements

The loss over a length of fiber, L_1 (typically 2-3 m) was measured. The fiber was then cut-back a number of times (e.g. in 20 cm segments, L_2, L_3) and the output power, P, measured each time. The attenuation value was calculated through a linear least square fitting of the experimental data.

3.4.2 Laser Performance

Within the research group, laser emission of the active fibers fabricated in this work was demonstrated by Dr. Joris Lousteau and Mr. Gerardo C. Scarpignato. In Figure 3.11, the experimental set up is shown.

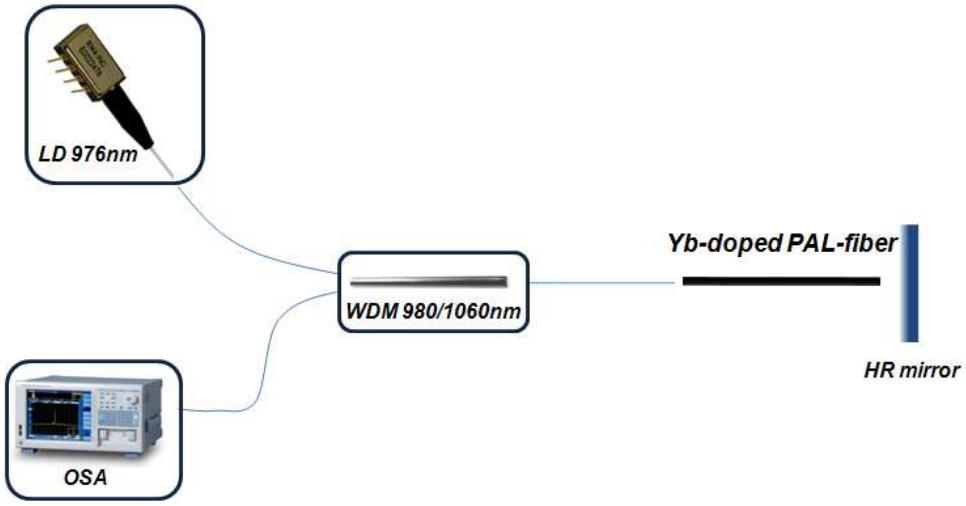

Figure 3.11: Scheme of the experimental set-up for laser emission demonstration

The main components used for the experimental setup are the laser diode

pump at a wavelength of 976 nm, the wavelength division multiplexing combiner (operating at 980/1060 nm); the HR mirror, the Optical Spectrum Analyzer and the computer with GPIB interface. In order to form the cavity the active PAL-fibers were carefully attached to an aluminium separator while taking care to maintain the fiber parallel to the groove in the fiber holder. Afterwards, the separator was fixed by tightening the corresponding screw. To adjust the HR mirror with the active fiber, the first one was finely moved until both components were in contact, fact that was confirmed by observing that both components began to displace together. The mirror was not fixed. Once the resonance cavity was conformed, the WDM output fiber end was butt-coupled to it. A preliminary alignment was carried out using a 3-axis micropositioner and a microscope located above the component assembly. The optimal position was achieved by maximazing the output power peak present in the OSA spectrum. The pump laser current (iL) was varied in order to characterize the Yb-doped fiber output power in relation to the pump laser power (P_L), and as a consequence, the launched pump power (Pp) entering into the fiber.

BIBLIOGRAPHY

1. N. El-Shafi, S. Ibrahim, A. Ali, “Chemical durability of some P_2O_5-PbO-Al_2O_3-R_2O glasses”, in *Physics and Chemistry of Glasses –European Journal of Glass Science and Technology part B* 50(1), 45-51,(2009).
2. C. R. Kurkjian, “Mechanical properties of phosphate glasses” Journal of Non-Crystalline Solids 263-264, 207-212 (2000).
3. M. Karabulut, E. Melnik, R. Stefan, G. K. Marasinghe, C. S. Ray, C. R. Kurkjian, and D. E. Day, “Mechanical and structural properties of phosphate glasses” in *Journal of Non-Crystalline Solids* 288, 8-17 (2001).
4. J.D. Myers and C.S. Vollers, US Patent 4 248 732 (1981).
5. http://www.metricon.com/
6. M. Yamane and Y. Asahara, Glasses for Photonics, Cambridge University Press, (2004).

Chapter 4

Fiber Fabrication

In this chapter are reported and discussed the results on the different fabrication methods of the phosphate glasses prepared and characterized within this research work. The resulting fibers are also described, focusing on the fabrication method of preforms and subsequent fiber drawing process. A step by step study and analysis of the different problems, optimization on the material and/or on the process were carried out in order to improve the quality of the fabricated glasses and therefore the performance of manufactured fibers.

The chapter is divided into 5 sections. The first section (4.1) concerns the description of the single cladding fiber obtained from a first set of phosphate glasses, with the purpose studying the behavior of the prepared glasses and the feasibility of the process. The second section (4.2) covers a study of the feasibility of a double cladding fiber, based on the optimization of the glasses previously studied. In the third section (4.3) the fabrication of a first active double cladding fiber is reported, based on a core glass doped with Yb_2O_3. In the third session is also reported a single cladding fiber obtained by the same doped glasses, manufactured as a test in order to study and understand the performance of the fabricated materials and the fibers. The fourth paragraph (4.4) reports a second active double cladding fiber doped with different amount of Yb_2O_3, obtained from the glasses manufactured with a new method and different precursors, with the aim to improve the quality and the reproducibility of the

glasses in terms of refractive index variations. The fifth (4.5) section reports the fabrication of a double cladding fiber with a low numerical aperture of the core, obtained from glasses produced with a manufacturing method designed to have a complete control between the difference of refractive index between the core and the first cladding.

4.1 Single Cladding Passive Fiber (*PALSC-01*)

a) Glass fabrication and characterization

Four different glasses (PAL 01, 02, 03, 04) were studied for the first fiber drawn in this work. The samples were named as “PAL” after the initial of the main constituents: PAL_{01}, for the core; PAL_{02} to PAL_{04} as candidates for the cladding glass. The glasses were fabricated with Method 1 (section 3.1.1 of the Chapter 3). The reagents (30g), weighed in a glove box, have been fused in alumina crucibles. The temperature schedule has been set as follows:

Initial Temperature [℃]	Final Temperature [℃]	Dwell Time [min]
20	300	60
300	1400	60
1400	1600	60
1600	1400	60

For all ramps was used a rate of 15° C/min. The melting process was carried out by blowing 3 l/min of a mixture of dry N_2/O_2 into the furnace. The melt

was then cast in a brass plate pre-heated at a temperature of 400° C. The so-obtained glass was annealed at 460℃ for 5h to remo ve any thermal stress. The glass sample was then cooled down slowly at room temperature. Clear and homogenous glasses were cast and characterized for all compositions.

In order to obtain the desired refractive index contrast between the core and the cladding, the amount of Li_2O was gradually increased (in substitution of BaO) moving from PAL_{01} to PAL_{04}. This change was justified by the different atomic weights and polarizabilities of the Li^{2+} and Ba^{+} ions. In detail, the polarizability and the mass of the Li^{2+} ion are lower than the corresponding polarizability and mass of the Ba^{+} ion. Therefore, when BaO is replaced by Li_2O, the lower atomic weight of the metal causes a decrease in the electronic density and polarizability of the glasses and thus a decrease in the refractive index (see Table 4.1) as predicted by the Lorenz-Lorenz equation [1]. The decrease of the measured refractive index moving from sample PAL_{01} to PAL_{04} is clearly evident in Figure 4.1.

Table 4.1: Refractive index values for the PAL_{01}, PAL_{02}, PAL_{03} and PAL_{04} samples measured at different wavelength (accuracy of the measurements was estimated to be ± 10^{-3})

Sample	633 nm	825 nm	1016 nm	1316 nm	1533 nm
PAL_{01}	1.558	1.552	1.549	1.547	1.544
PAL_{02}	1.552	1.548	1.545	1.542	1.538
PAL_{03}	1.550	1.545	1.543	1.540	1.537
PAL_{04}	1.548	1.542	1.539	1.537	1.534

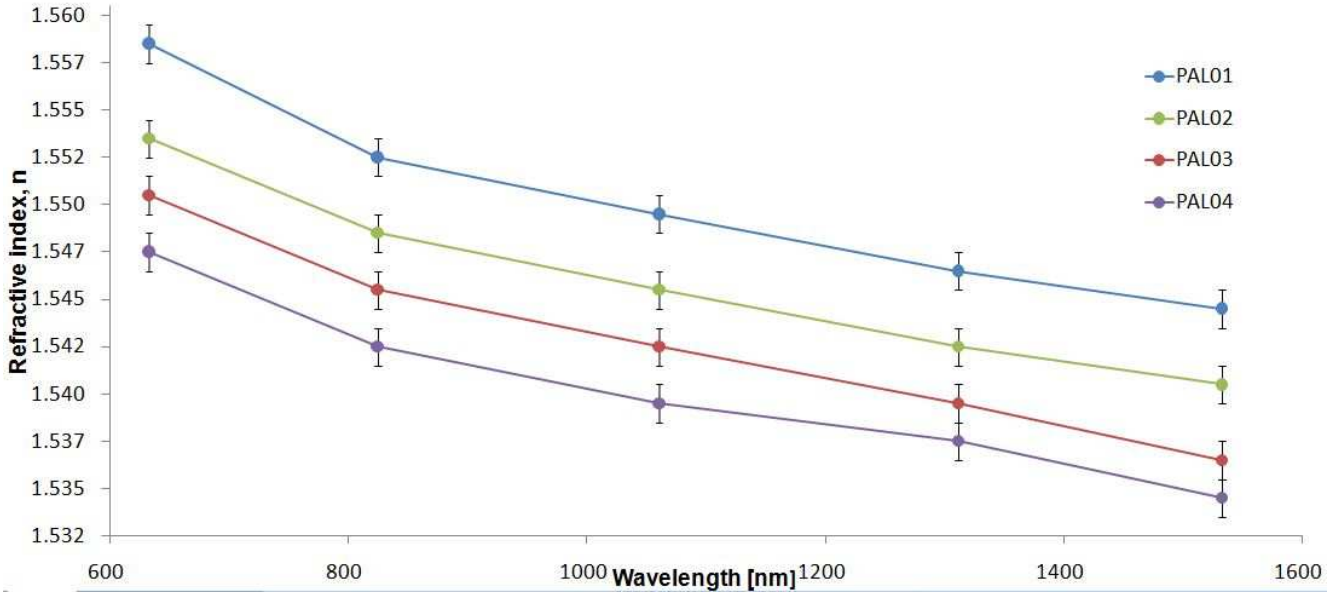

Figure 4.1 - Plot of refractive index values of PAL_{01}, PAL_{02}, PAL_{03} and PAL_{04} glasses at different wavelenght

The values of the numerical apertures (NA) calculated on the basis of the refractive indices measured at the wavelength of 1016 nm are shown in Table 4.2. The NA values range from 0.11 to 0.17 for the different glass pairs.

Table 4.2: Numerical Aperture values for the PAL_{01-02}, PAL_{01-03}, PAL_{01-04} pairs calculated at 1016 nm

Sample	NA
PAL_{01-02}	0.11
PAL_{01-03}	0.14
PAL_{01-04}	0.17

Table 4.3 shows the glass transition temperature (T_g), the onset of crystallization (T_x) and the corresponding glass stability parameter ($\Delta T = T_x - T_g$) of

the fabricated glasses. A random error of ±3 ℃ was observed in measuring these temperatures. All the fabricated glasses fabricated show great stability against crystallization. The glass stability parameter was found to be higher than 200° C for all samples. The transition temperature of PAL-glass systems increases with BaO content and, consequently decreases with increasing the amount of Li_2O.: this trend is likely related to the increase inside the glass of non-bridging oxygen sites (NBO). The increase of the molar concentration of (Li_2O) creates a weaker structure of the phosphate glass because, network modifiers act as non-bridging oxygen formers. On the other hand, the observed great stability (ΔT) is mainly due to the high concentration of network intermediates (B_2O_3, Al_2O_3 and La_2O_3) that reinforce the structure and raise the crystallization temperature [2].

Table 4.3: Glass transition temperature (T_g), onset of crystallization (T_x) and glass stability (ΔT) for the PAL_{01}, PAL_{02}, PAL_{03} and PAL_{04} sample

Sample	T_g [℃] ±3	T_x [℃] ±3	ΔT [℃] ±6
PAL_{01}	477	690	213
PAL_{02}	475	701	226
PAL_{03}	473	674	201
PAL_{04}	468	675	207

b) Preform fabrication

After this preliminary study on the material, the following activity was focussed on the study of the preform fabrication process. From the results of the thermal and optical properties, the compositions selected for the fabrication of the preform were: PAL_{01} for the core and PAL_{04} for the cladding. The first step for the preform fabrication was to manufacture the core rod. The parameters of the

process were studied and optimized for the selected composition in order to obtain a rod free of bubble and cracks. PAL_{01} glass selected for the core was melted and poured into a pre-heated brass mold to produce a 10 cm long rod with a diameter of 1 cm. After 48 h annealing at 460℃, the rod core was carefully polished to an optical quality with SiC paper of different grits (from 100 down to 4000).

In-house built-up equipment was used to fabricate the cladding tube by rotational casting technique (see Chapter 3, Section 3.3.1). Numerous trials of tubes were carried out in order to optimize the rotational casting process. The performed tests were intended to control the parameters such as mould temperature, glass quenching temperature, rotational speed, etc. to process a tube without defects along the length of the preform:

- ***Mold temperature*** too high, the cast glass of the cladding tube can get stuck to the walls of the mold, via thermal reaction. On the other hand, if the temperature of the mould is too low, the cast glass cracks, via thermal shock.
- ***Casting temperature***, if too high, the cast glass sticks to the mould and easily cracks. While, if the casting temperature is too low the cast tube diameter will not be constant along the entire length, and in some cases the tube will not be obtained in the desired extension.
- ***Rotational speed*** affects primarily the dimension and the homogeneity of the internal diameter of the tubes.it was necessary to study and adapt them to each other.

The variables of the process were hence evaluated and optimized for the selected composition (PAL_{04}) in order to obtain glass cladding tubes with controlled and reproducible internal diameter.

After annealing at 460℃ for 48 h, the outer surface of the cladding tube was polished with SiC paper of different grits (from 100 down to 4000). In the meantime the core rod was then stretched on the drawing tower to reduce its diameter, in order to fit into the cladding tube.

c) Fiber drawing and characterization

The preform was heated in an in-house developed drawing tower by using a RF induction heating system (SAET, Torino, Italy). A temperature between T_g and T_x is necessary to draw the fiber through a cylindrical ring graphite susceptor. The fiber diameter was monitored during the drawing. Typical values of the drawing process were: a drawing temperature around 600° C, and a drawing speed of 3 m/min. More than 200 m of single cladding phosphate fiber, named PAL-SC01, were drawn with a constant external diameter of (125±1) μm and a core diameter of (40±1) μm. Through the calculation of the V number is evident that the fiber is highly multimode (see Chapter 2, Section 2.1). In fact, for the values of refractive indexes and core size of the PALSC-01 fiber, the V-number at 1016 nm is equal to: 41.

During the drawing process, a series of scattering centers were evident along the drawn fiber, probably due to an initial process of crystallization. An optical micrograph of the fabricated optical fiber cross-section is shown in Fig. 4.2(a) where the circular and concentric core is evident. The step-index between the core and the cladding is also evident by the brighter coloration of the

centered core compared to the cladding. Using a single mode fiber pigtailed laser at the wavelength of 1310 nm, the near field image of the fiber output beam was collected by an IR video-camera reported in Figure 4.2(b).

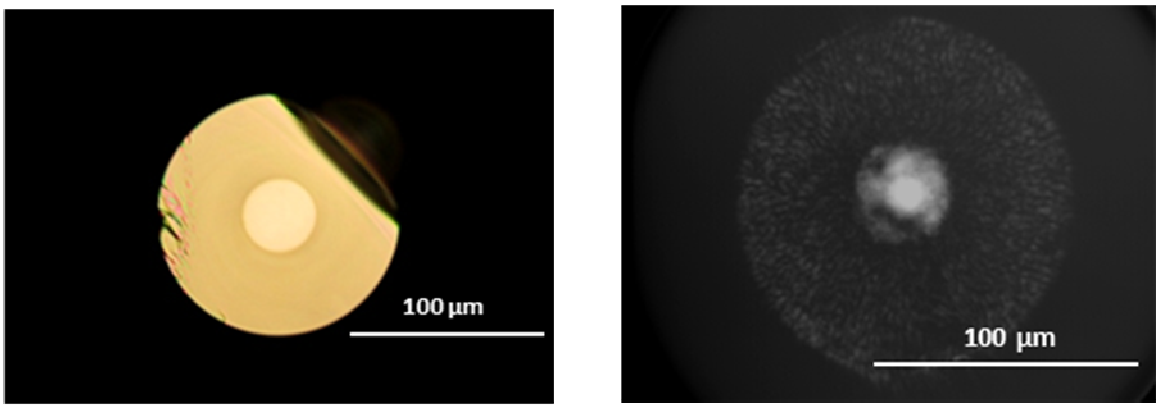

(a) (***b)***

Figure 4.2 - Photograph of the produced PALSC-01 phosphate optical fiber taken by optical microscope (a) and image of the near field (b) of the optical fiber taken by launching light at the wavelength of 1310 nm

Cut-back loss measurements were performed on the PALSC-01 fiber (see Chapter 3, Section 3.4.1). The initial length of the section of the fiber analyzed was 2 m. The attenuation value was calculated through a linear least square fitting of the experimental data as reported in Figure 4.3. The attenuation loss at 1300 nm was measured to be 7.30 dB/m. This values is relatively high when compared to the values reported in literature for the phosphate fibers (3 dB/m) [3].

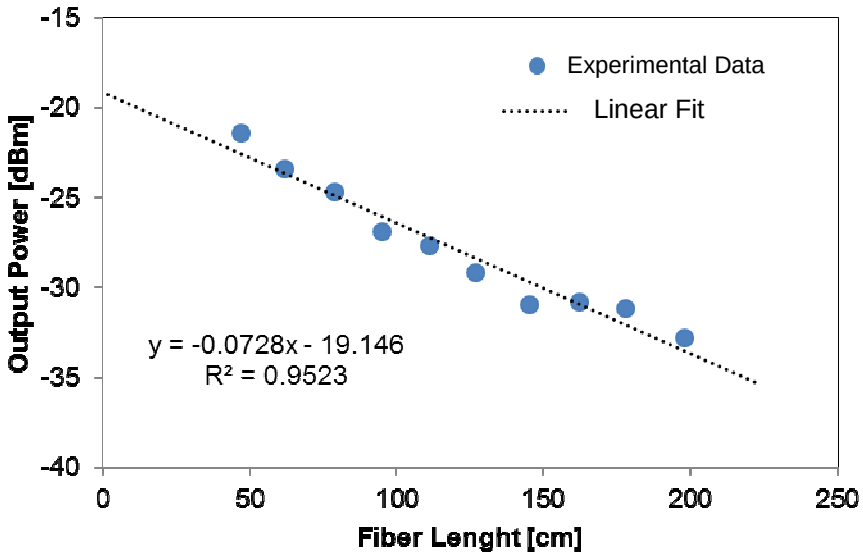

Figure 4.3 - Attenuation losses of the PALSC-01 phosphate optical fiber at 1300 nm

The high attenuation loss value of the PALSC-01 fiber is mainly due to scattering effects and is related with the small crystallized particles created during the drawing process. The origin of the crystals was explained with the high temperatures (1600° C for 1h) used during the fabri cating process of the performs: the high temperature caused the incorporation of impurities from the crucibles, such as alumina particles which acted as nucleation centres thus promoting crystallization processes during fiber drawing. As solution, the reduction of the melting time and temperature was decided for future glass samples.

Starting from the test study on the materials and the process to produce the *PALSC-01* fiber, the attention was then focussed on the design and optimization of the glasses for the fabrication of the double cladding fiber configuration.

4.2 Double Cladding Passive Fiber

(*PALDC-01*)

a) Glass fabrication and characterization

Starting from the previous PAL-compositions, three phosphate glass compositions were designed and studied for the fabrication of the double-cladding fiber. The samples were named as: PAL_{05}, for the core glass; PAL_{06} as candidates for the first cladding; and PAL_{07} as candidate for the second cladding glass. The glasses for the fabrication of the phosphate double-cladding fiber were produced by using Method 2 (see Chapter 3, Section 3.1.1,). The reagents (30g), weighed in a glove box, have been fused in alumina crucible. The temperature schedule has been set as follows:

Initial Temperature [℃]	Final Temperature [℃]	Dwell Time [min]
20	300	60
300	1350	45
1350	1500	60

For all ramps was used a rate of 15° C/min and all melting were carried out by blowing 3 l/min of a mixture of dry N_2/O_2 into the furnace. The glass melt was then cast in a pre-heated brass plate at a temperature of 400℃. The formed glass was annealed at 470℃ for 5h to remove any th ermal stress. The glass sample was then cooled down slowly at room temperature.

In order to maintain an adequate numerical aperture between the core and

the first cladding and between the first and the second cladding (NA>0.40), while preserving similar thermo-mechanical properties, the addition of PbO was necessary into the core (PAL_{05}) and first cladding compositions (PAL_{06}) in different amounts. On the other hand, to decrease the refractive index value, the second cladding composition (PAL_{07}) was modified by adding MgO, while BaO and La_2O_3 were completely removed. These changes in the compositions were reflected in a substantial variation of the indices of refraction compared to the glasses previously studied (PAL_{01}-PAL_{04}). In Table 4.4 the refractive index values of the prepared samples are shown. The introduction of the heavy and highly polarizable PbO in the core (PAL_{05}) and the first cladding (PAL_{06}) glasses resulted in an increase in the refractive index values. The absence of BaO and La_2O_3, replaced by different amounts of Li_2O, Al_2O_3 and MgO, in the second cladding glass (PAL_{07}) caused a significant decrease of refractive index to 1.505 measured at wavelength of 1533 nm.

Table 4.4: Refractive index values for the PAL_{05}, PAL_{06}, and PAL_{07} samples measured at different wavelength (accuracy of the measurements was estimated to be ± 10^{-3})

Sample	633 nm	825 nm	1016 nm	1312 nm	1533 nm
PAL_{05}	1.583	1.577	1.573	1.570	1.567
PAL_{06}	1.580	1.573	1.569	1.565	1.563
PAL_{07}	1.526	1.520	1.516	1.513	1.510

The values of numerical aperture (NA) calculated on the basis of the refractive indices measured at 1016 nm are reported in table 4.5.

Table 4.5: Numerical Aperture values for the PAL_{05-06} and PAL_{06-07} pairs calculated at 1016 nm

Sample	NA
PAL_{05-06}	0.12
PAL_{06-07}	0.40

Table 4.6 shows the glass transition temperature (T_g), the onset of crystallization (T_x) and the glass stability ($\Delta T = T_x - T_g$) of the produced glasses. For all three samples, more than 190°C of difference between the T_x and T_g were found.

Table 4.6: glass transition temperature (T_g), onset of crystallization (T_x) and glass stability (ΔT) for the PAL_{05}, PAL_{06} and PAL_{07} sample

Sample	Tg [℃] ±3	Tx [℃] ±3	ΔT [℃] ±6
PAL_{05}	490	705	215
PAL_{06}	485	675	190
PAL_{07}	479	669	190

b) Preform fabrication

The first step for the preform fabrication was to manufacture the core rod. The glass selected for the core (PAL_{07}) was melted and then poured into a pre-heated brass mold to produce a 10 cm long rod with a diameter of 1 cm. The core rod was then placed inside the annealing furnace for 48 h at 470℃. The core rod was carefully polished with SiC paper of different grits (from 100 down to 4000). The cladding tubes were fabricated by rotational casting technique (see Chapter 3, Section 3.3.1). Different tests were performed in order to optimized the

rotational casting parameters for the different compositions: PAL_{06} and PAL_{07}. The variables of the process (rotation speed and time, casting temperature and mold temperature) were consequently evaluated and optimized in order to obtain glass cladding tubes with controlled and reproducible internal diameter.

After annealing at 470℃ for 48 h, the outer surface of the cladding tube was polished with SiC paper of different grits (from 100 down to 4000). In the meantime, the core rod was then stretched on the drawing tower to reduce its diameter, to fit into the first cladding tube. After this first stretching, the core/first cladding structure was stretched to reduce its diameter and so it was introduced into the second cladding tube.

c) Fiber drawing and characterization

The preform was heated in drawing tower by using the induction heating system to reach a temperature between T_g and T_x to draw the fiber through a cylindrical ring graphite susceptor. The fiber diameter was monitored upon drawing. Characteristic parameters of the drawing process were: drawing temperature around 600° C, and drawing speed of 3 m/min.

More than 200 m of double cladding phosphate fiber, PAL-DC01, were drawn with a constant external diameter of (125±1) μm, an inner cladding diameter of (35±1) μm and a core diameter of (10±1) μm. The calculated V number of the PALDC-01 fiber at 1016 nm is 3.3, which means that the fiber supports few modes. An optical micrograph of the fabricated optical fiber cross-section is shown in Fig. 4.4(a) where a slight deformation of the first cladding is evident This misalignment of the first cladding is due to a not constant inner diameter along the length of the second cladding. The step-index between the

different parts of the fiber is evident by the different brightness in the cross section. Using a single mode fiber pigtailed laser at the wavelength of 1310 nm, the near field image of the fiber output beam was collected by an IR video-camera reported in Figure 4.4(b). A series of scattering centers were evident along the drawn fiber during the drawing process, probably due to an initial process of crystallization.

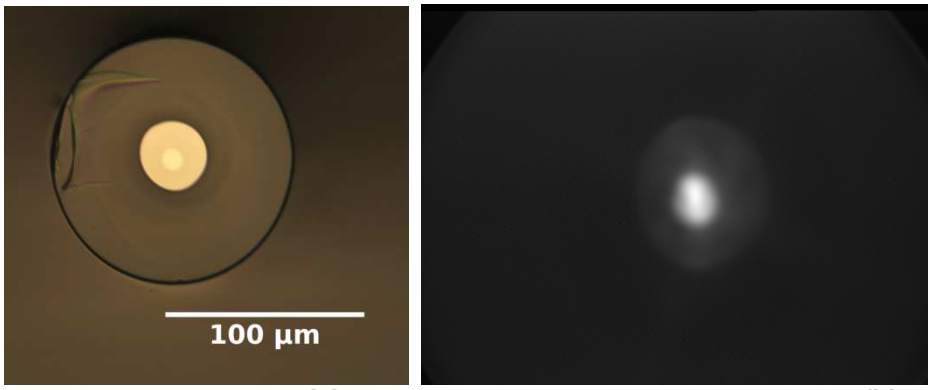

(a) **(b)**

Figure 4.4 - Photograph of the produced PALDC-01 phosphate optical fiber taken by optical microscope (a) and image of the near field (b) of the optical fiber taken by launching light at the wavelength of 1300 nm

Cut-back loss measurements were performed on the PALDC-01 fiber. The initial length of the section of fibre analyzed was about 2 m. The attenuation value was calculated through a linear least square fitting of the experimental data as reported in Figure 4.5. Attenuation loss at 1300 nm was measured to be 11.0 dB/m.

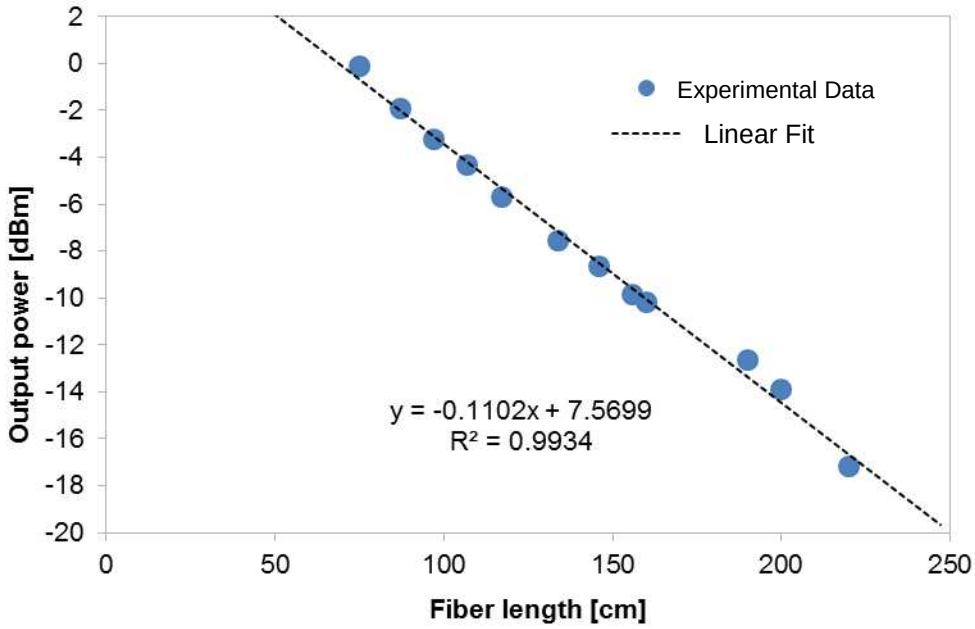

Figure 4.5 - Attenuation losses of the PALDC-01 phosphate optical fiber at 1300 nm

Despite the change in the manufacturing parameters (T, t melting), the attenuation losses are increased. The melting temperature was in fact set for these glasses at 1500° C for only 15 min, instead o f 1600° C for 1h as for the previous method, but this was not enough to solve the problem of crystallization due to impurities. In addition, the values of attenuation losses in the fiber PALDC-01 are related with problems at various interface of the fiber: core-first cladding and first cladding-second cladding respectively (particles, impurities, surface imperfections). To improve the performance of the fibers and reduce the attenuation loss, a potential solution was to change manufacturing parameters (further reduction of the temperature and time of glass melting) and an improvement of the quality and repeatability of the cleaning and polishing process of preforms (for both cladding tubes and core rod).

4.3 Yb-doped (3.45mol% Yb_2O_3) Double Cladding Fiber (*PALYb-01*)

a) Glass fabrication and characterization

After the preliminary study on the materials and process related to the manufacture of passive fibers (PALSC-01 and PALDC-01), the work was focused on the study of doped glasses with the aim of fabricate active fibers. For the first active fiber, a molar concentration of Yb_2O_3 equal to 3.45mol% was chosen, which it is equivalent to a weight concentration of about 9wt%. The Yb^{3+} ion density of the prepared glass was calculated (Equation 3.10) and it was found to be equal to 8.0 x 10^{20} ions/cm^3. The sample Yb_{01} was prepared by replacing in the sample PAL_{05} (passive core) La_2O_3 for Yb_2O_3, (3.45mol%). The samples prepared for the active fiber were obtained by decreasing the melting temperature and time of Method 2. The melting temperature was in fact set to 1400 °C for 15 min, for both melting steps, instea d of the previous 1500°C.

In Table 4.7 are reported the refractive index values for the Yb_{01} sample at different wavelength. As clear by the measurements of refractive index, this change in the composition (Yb_2O_3 for La_2O_3) resulted in a reduction of the refractive index of the doped sample. This is probably due to the different polarizabilities of the two oxides: Yb_2O_3 against La_2O_3 [4]. As a consequence of this lowering, it was necessary to modify the composition of the first cladding (PAL_{06}) by replacing 2% of PbO with an equal amount of Li_2O, to decrease the value of its refractive index. The name of the new sample is PAL_{08}. The values of numerical aperture (NA) calculated on the basis of the refractive indices

measured at 1016 nm are equal to 0.16 and 0.37, respectively for the core/first cladding and for the first cladding/second cladding pairs.

Table 4.7: Refractive index values for the Yb_{01}, PAL_{08} and PAL_{07} samples measured at different wavelength (accuracy of the measurements was estimated to be ± 10^{-3})

Sample	633 nm	825 nm	1016 nm	1316 nm	1533 nm
Yb_{01}	1.579	1.573	1.569	1.565	1.563
PAL_{08}	1.569	1.563	1.560	1.557	1.555
PAL_{07}	1.526	1.520	1.516	1.513	1.510

Table 4.8 shows the glass transition temperature (T_g), the onset of crystallization (T_x) and the glass stability ($\Delta T = T_g - T_x$) of the samples studied for the fabrication of the Yb-doped fiber. All the fabricated samples show great stability against crystallization (ΔT).

Table 4.8: Glass transition temperature (Tg), onset of crystallization (Tx) and glass stability (ΔT) for the Yb_{01}, PAL_{08}, and PAL_{07} samples

Sample	Tg [℃]±3	Tx [℃]±3	ΔT [℃]±6
Yb01	489	672	183
PAL_{08}	481	675	194
PAL_{07}	479	669	190

The sample Yb_{01} was also studied with UV-Vis spectroscopy. In Figure 4.4 is shown a spectrum of the absorption cross section of the Yb_{01} glass.

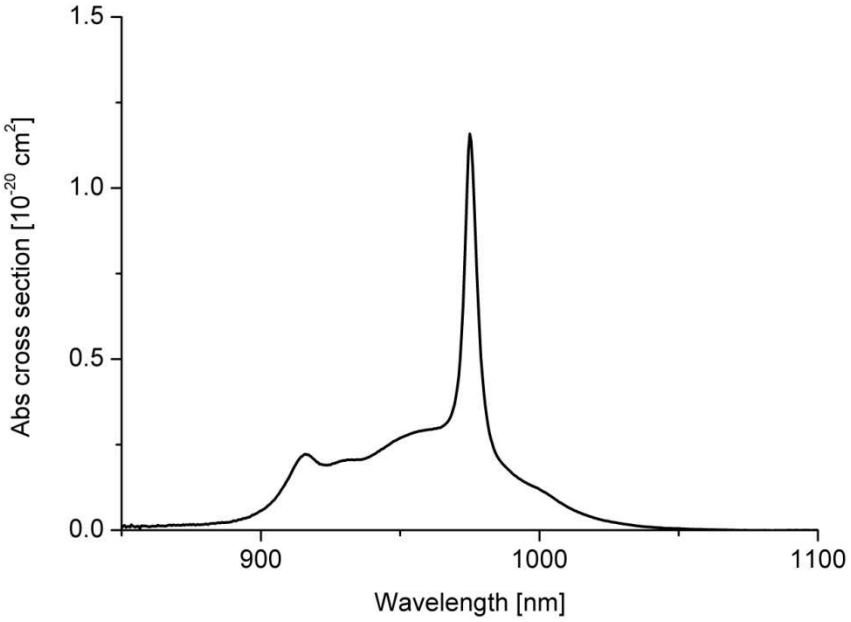

Figure 4.6 – Absorption cross section of the Yb_{01} sample

The absorption cross section was then calculated through analysis of the UV-Vis spectra (Chapter 3, Section 3.2.4). The value of calculated cross section at 975 nm was equal to: $1.25x10^{-20}$ ion/cm^3, and it is in good agreement with values reported in literature [5,6] The lifetime of Yb^{3+} ions in the glass Yb_{01} was measured and calculate as illustrate in Chapter 3, Section 3.2.5. The value of lifetime in Yb_{01} was found equal to: (1.5±0.1) ms. This value is in good agreement with other values of lifetimes reported in the literature for glasses with similar Yb^{3+} ion concentrations of the sample Yb_{01} concentration [7].

b) Preform fabrication

As for the previous fibers, for the manufacture of the preform the first step was to manufacture the rod with the composition Yb_{01}. While for the claddings were fabricated two tubes: one for the first (PAL_{08}) and one for the second (PAL_{07}) cladding respectively. The parameters used for the fabrication of the tubes of this fiber were the same parameters used for the manufacture of tubes of fiber PALDC-01. After the annealing, the individual parts that constitute the preform have been systematically cleaned and polished. Particular attention was given at cleaning and polishing rods and tubes, in order to minimize imperfections or impurities of contamination that weaken the fiber and increase the propagation loss. To this purpose, during the polishing process alumina suspensions of different size were used, as abrasives, as well as the SiC paper of different grits (from 100 down to 4000). At the end of the polishing process, the different parts of the preform were placed in hot ethanol and subsequently they were washed with hot acetone.

The core rod was then stretched on the drawing tower to reduce its diameter, to fit into the first cladding tube.

c) Fiber drawing and characterization

The preform was heated in the drawing tower to draw the Yb-doped double cladding phosphate fiber (PALYB-01). Characteristic values of the drawing process were: a drawing temperature around 600° C, and a drawing speed of 3 m/min. The fiber diameter was monitored during the drawing process. The dimensions of the PALYb-01 fiber are: (125±1) μm for the diameter of the outer

cladding, (25±1) μm for the diameter of the inner cladding and (7±1) μm for the diameter of the core. For those values of core size and refractive indexes the V-number at 1016 nm is equal to: 3.5. The fiber is in fact multi-mode (see Chapter 2, Section 2.1).

In Figure 4.7 are shown an optical micrograph of the fabricated optical fiber cross-section, and a near field image of the fiber. From the optical microscope image (a) is evident that core and first cladding are circular and concentric. The step-index between the core and the cladding is also evident by the brighter coloration of the formed compared to the second. The near field image of the fiber end face (b) shows light-guiding into the core.

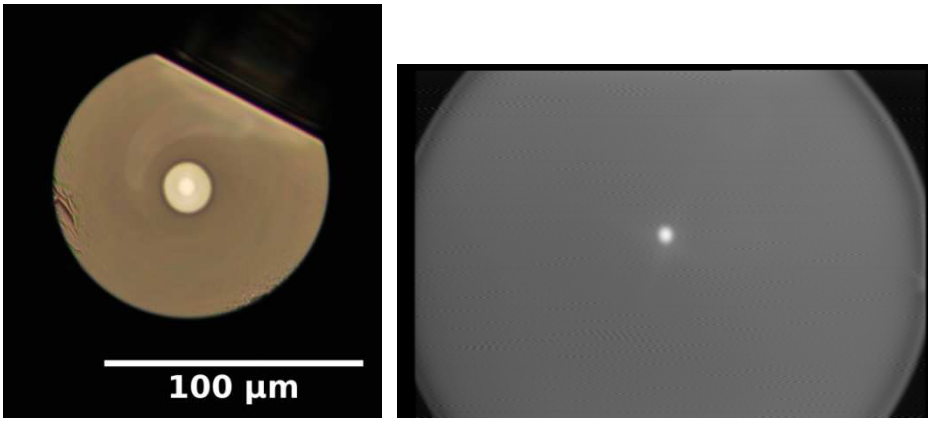

(a) (b)

Fig. 4.7 - Photograph of the produced PALYb-01 phosphate optical fiber taken by optical microscope (a) and image of the near field (b) of the optical fiber taken by launching light at the wavelength of 1310 nm

Also on the PALYb-01 fiber cut-back loss measurements were performed. The initial length of the section of fiber analyzed was 4 m. The attenuation value was calculated through a linear least square fitting of the experimental data as reported in Figure 4.8. Attenuation loss at 1300 nm was measured to be 7.50

dB/m.

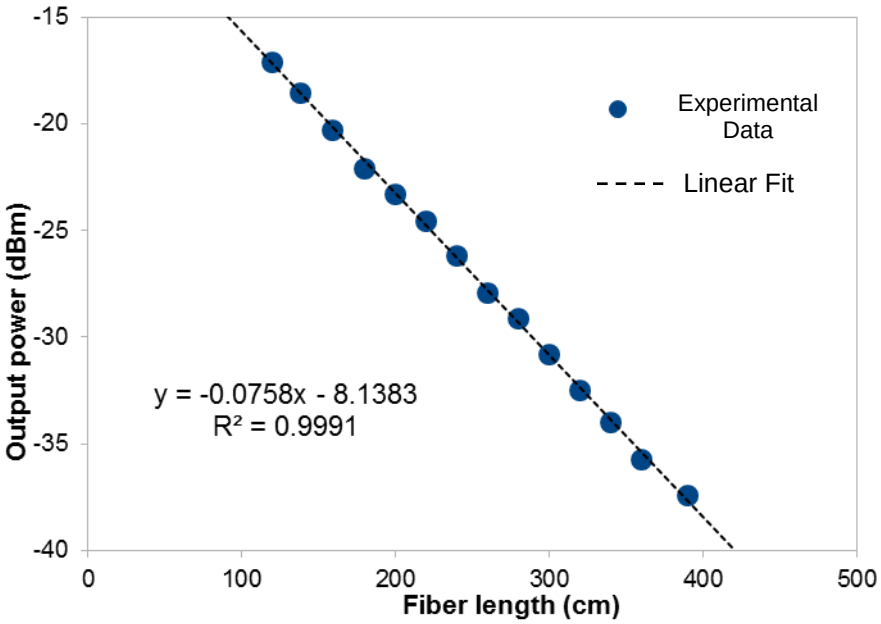

Figure 4.8 - Attenuation losses of the PALYb-01 phosphate optical fiber at 1300 nm

The values of attenuation losses of the active fiber PALYb-01 are lower than the values of losses of the previous double cladding passive fiber PALDC-01 (11.0 dB/m), but still comparable to the values of losses of the fiber PALSC-01. The attenuation losses are mainly due to scattering effects occurring into the fiber. The scattering effect here is even more pronounced in relation to the small dimensions of the core (7 µm for the core diameter).

To evaluate the values of attenuation losses due to intrinsic problems related to the fabricated materials, a test fiber was then pulled.

d) Single Cladding Test Fiber

(*PAL-test*)

In order to assess the quality of the PAL-glasses and exclude intrinsic causes of attenuation loss due to the fabricated materials a test fiber, named PAL-test, was drawn and characterized.

The preform used for the fabrication of the fiber PAL-test was made of Yb_{01} glass for the core and PAL_{08} glass for cladding, the same glasses used in the fiber PALYb01. The fiber PAL-test presented, however, a single cladding structure. The single cladding fibre was drawn with the dimensions of: (125±1) μm for the diameter of the cladding and (40±1) μm for the diameter of the core, the same dimension as that for the fiber PALSC-01. As can be seen in figure 4.9(a), the core remained circular and concentric. No defects or bubbles are present at the core/cladding interface. The near field image of the fibre output beam was collected on an IR videocamera. A near field micrograph of the fibre end face illustrating guiding is shown in Figure 4.9(b).

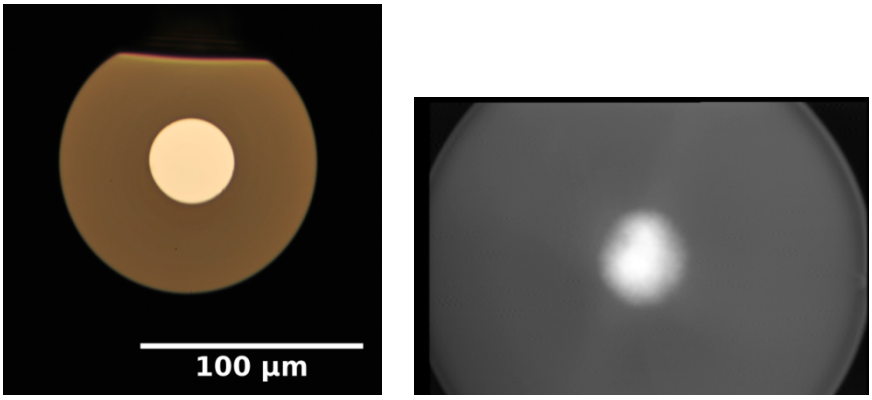

(a) (b)

Figure 4.9 - Photograph of the produced PAL-test phosphate optical fiber taken by optical microscope (a) and image of the near field (b) of the optical fiber taken by launching light at the wavelength of 1300 nm

The attenuation losses of the PAL-test fiber were studied by cut-back loss measurements. The initial length of the section of fibre analyzed was around 5 m. The attenuation value was calculated through a linear least square fitting of the experimental data as reported in Figure 4.10. Attenuation loss at 1300 nm was 2.0 dB/m.

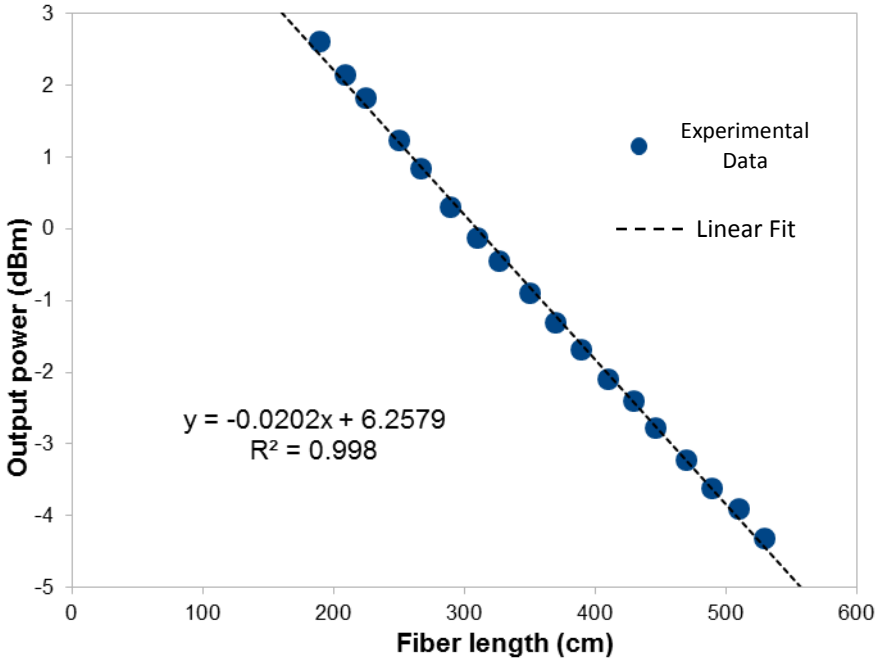

Figure 4.10 - Attenuation losses of the PAL-test phosphate optical fiber at 1300 nm

Although composed of the same glass, the values of attenuation loss of the fiber PAL-test are far lower than the values of the previous fiber (PALYb-01). After this test it is evident that, despite being of the same glasses, the light, confined in the fiber with a core diameter more than 5 times larger than the previous one, is transmitted with attenuation losses almost 4 times lower. Therefore the very high attenuation loss of the previous PAL-fibers fabricated are not related to intrinsic problems of the material. In addition, the PAL-test fiber presents attenuation losses values far lower than PALSC-01 (7.3 dB/m), with which it shares the same dimensions but different manufacturing processes and so different glasses. Thus the changes occurred in the process of glass and preform fabrication led to an improvement of the fabricated glasses and of the

performance of the produced fibers. Moreover, the attenuation losses values of the PAL-test fiber are 1 dB/m below the lowest attenuation values reported in literature for phosphate fibers [4].

4.4 Yb-doped (1.1mol% Yb_2O_3) Double Cladding Fiber (*PALYb-02*)

a) Glass fabrication and characterization

In this section the study of a new method of fabricating phosphate glass samples is reported and discussed: the aim was to improve the quality and the reproducibility of the glass in terms of refractive index variations. With the set of glasses obtained from this method a second active fiber (PALYb-02) was drawn and characterized.

The samples prepared for the PALYb-02 fiber were fabricated using Method 3, described in Chapter 3, Section 3.1. In detail, for this set of glasses, the glass-former phosphorus pentoxide (P_2O_5) was replaced by ($NH_4H_2PO_4$). This change has been made to have better control in the weighing process of chemicals and to minimize contamination by water present in the atmosphere. In fact, the phosphorus pentoxide is extremely hygroscopic and reacts immediately with the moisture, making difficult and long the weighing step. On the contrary the ammonium di-hydrogen phosphate is a stable compound and forms P_2O_5 only at high temperature. The fabrication procedure of this set of glasses consisted in a treatment in alumina crucible. Inside the alumina crucible, the precursor ($NH_4H_2PO_4$) alone was pre-heated at 250° C for 2h while blowi ng 5 l/min of N_2

into the furnace. Then the remaining chemicals, weighted in a glove box under dried air atmosphere, was added into the crucible and the furnace temperature was raised up to 500° C 2°/min, to eliminate all th e gases produced during the heating (in particular ammonia). The temperature was then raised up to 1350° C and held for 30 min. Finally, the temperature of the furnace was raised up to 1400° C for 15 min and the glass was cast. All the process was carried out by blowing a mixture of N_2/O_2 into the furnace. The molten glass was cast in a pre-heated brass plate and then annealed at 480° C for 5h.

The molar concentration of Yb_2O_3 in the core was equal to a molar concentration of 1.1%. This molar concentration is equivalent to a weight percentage of about 2.9 % and an ions density equal to 2.6 x 10^{20} ions/cm^3.

In Table 4.9 the refractive index values for the prepared samples are reported: Yb_{02} for the core; PAL_{09} for the first cladding and PAL_{10} for the second cladding. As evidenced by the measures, the samples prepared with this new process have a slightly lower refractive index with respect to the previously prepared samples. In detail, samples PAL_{09} and PAL_{10^*} have refractive indices lower than the PAL_{06} and PAL_{07}, which respectively have the same composition. The values of numerical aperture (NA) calculated on the basis of the refractive indices measured at 1016 nm are equal to 0.18 and 0.39, respectively for the core/first cladding and for the first cladding/second cladding pairs.

Table 4.9: Refractive index values for the Yb_{02}, PAL_{09}, and PAL_{10} samples

measured at different wavelengths (accuracy of the measurements was estimated to be ± 10^{-3})

Sample	633 nm	825 nm	1016 nm	1316 nm	1533 nm
Yb_{02}	1.582	1.576	1.572	1.569	1.566
PAL_{06*}	1.571	1.565	1.561	1.558	1.555
PAL_{07*}	1.519	1.514	1.511	1.508	1.505

The lifetime of Yb^{3+} ions in the glass Yb_{02} was measured and calculated as illustrated in Chapter 3, Section 3.2.5.The value of lifetime in Yb_{02} was found to be equal to: (1.4±0.1) ms.

b) Preform fabrication

The fabrication process of the preform follows the steps described previously. The core glass (Yb_{02}) was melted and then poured into a pre-heated brass, while the cladding tubes were fabricated by rotational casting technique. The parameters used for the fabrication of the tubes of this fiber were the same parameters used for manufacturing the tubes of PALDC-01 fiber. After annealing at 480℃ for 48 h, the core rod and the cladding tu be were carefully polished with SiC paper of different grits (from 100 down to 4000) and suspensions of alumina. Despite the prolonged and careful polishing of the parts of the preform, the tubes and the rod showed a slight yellow/brown coloring, probably due to contamination of the platinum crucible (coloration not shown systematically by all the different glasses prepared with this method) [8]. This high contamination of Pt can be derived from a contact of the platinum with ammonia coming from the first fusion of the precursor ($NH_4H_2PO_4$) which releases ammonia. Nevertheless, the preform

was assembled as follows: the core rod was stretch on the drawing tower and fit into the first cladding tube; after that, a second stretch was performed on the core/first cladding structure to reduce its diameter and so it was introduced into the second cladding tube.

c) Fiber drawing and characterization

From the fabricated preform the PALYb-02 fiber was drawn. The dimensions of the PALYb-02 fiber are: (100±1) μm for the diameter of the outer cladding, (35±1) μm for the diameter of the inner cladding and (9±1) μm for the core diameter. Typical values of the drawing process were: a drawing temperature of about 600°C, and drawing speed of 3 m/min.

An optical micrograph of the fabricated optical fiber cross-section is shown in Figure 4.11(a) where the step-index between the core and the different claddings is evident by the brighter coloration of the center (core) compared to the outer parts of the cross section. The core and the first cladding are slightly off center. This misalignment is due to a not constant inner diameter along the length of the second cladding.

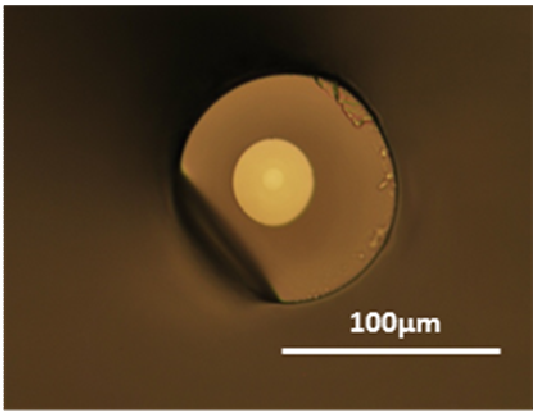

Figure 4.11 - Photograph of the produced PALYb-02 phosphate optical fiber taken by optical microscope

Cut-back loss measurements were performed on the PALYb-02 fiber. The initial length of the section of fiber analyzed was 1.5 m. The attenuation value was calculated through a linear least square fitting of the experimental data as reported in Figure 4.12. Attenuation loss at 1300 nm was 18.2 dB/m.

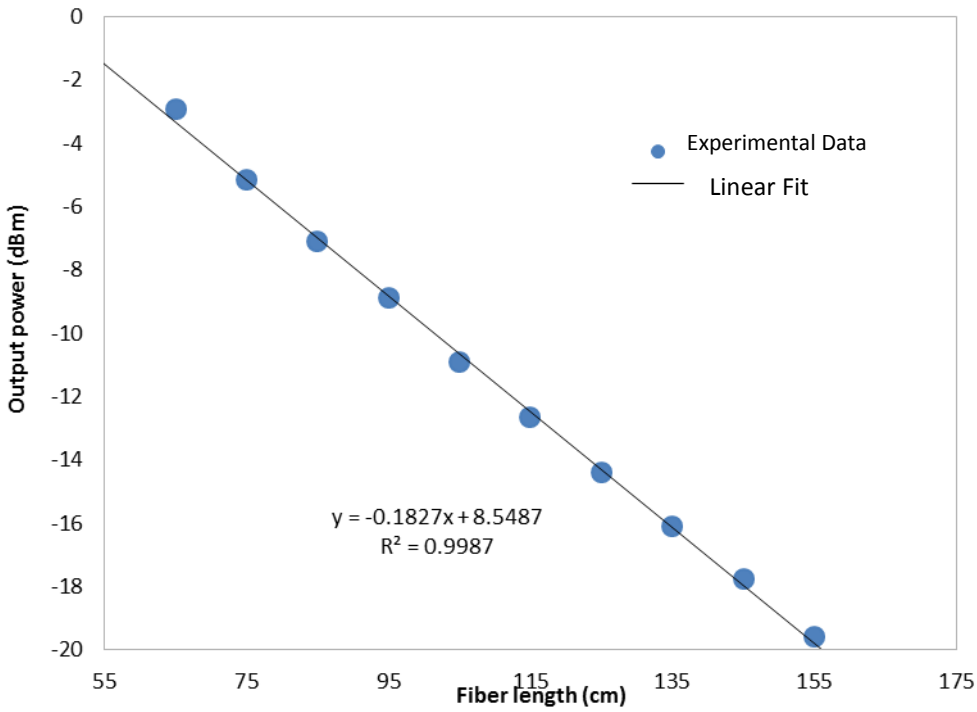

Figure 4.12 - Attenuation loss of the PALYb-02 phosphate optical fiber at 1300 nm

When compared with the previous measures, the high values of losses of the PALYb-02 fiber suggest problems resulting from the new fabrication process combined with the new precursor. This hypothesis is also confirmed by the yellow/brown coloration found in the glasses, coloration to be related to high contamination of Pt from the crucible, as also reported in [8].

In Figure 4.13 the comparison of refractive index values of nine phosphate glass samples prepared with Method 2 and Method 3 is reported. As evident, this fabrication process (Method 3) has led to a better control on the variations of the refractive index. The reproducibility of n for glass samples fabricated with Method 3 is in the order of 10^{-3}.

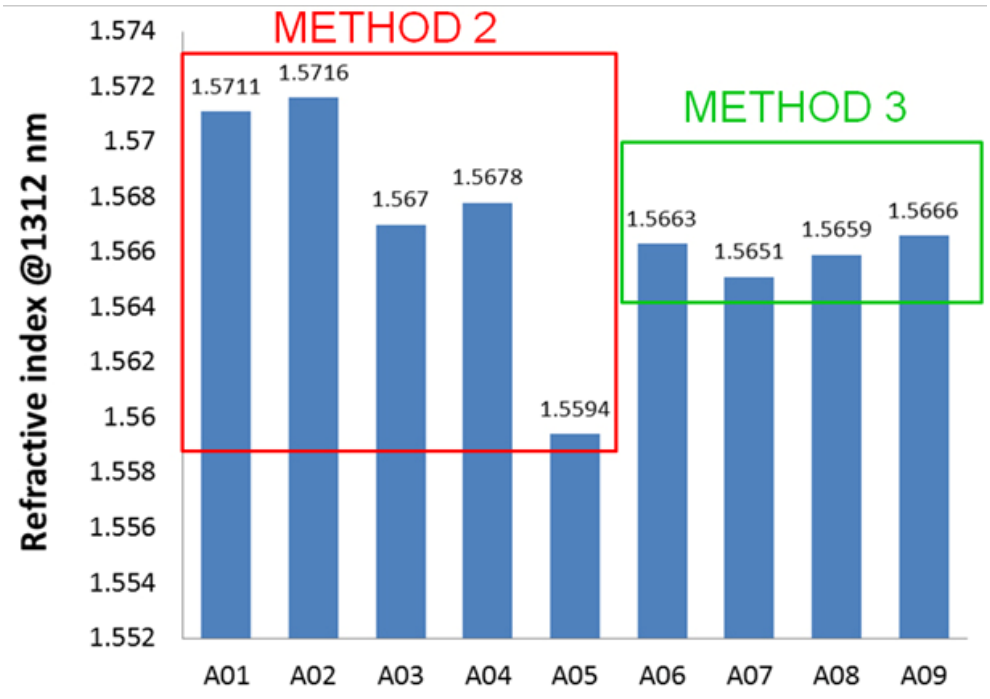

Figure 4.13 – Comparison of refractive index variations of glass samples prepared with Method 2 and Method 3

Nevertheless, from the measurements carried out on the fiber PALYb-02 it is clear that the use of the reagent $NH_4H_2PO_4$ as a precursor of P_2O_5 leads to the fabrication of glass not suitable for the use in optical field and in particular for use as optical fibers. So it was decided to cover another method of glass manufacture and abandon of the $NH_4H_2PO_4$ as a chemical precursor for the phosphate glass samples.

4.5 Yb-doped (1.1mol% Yb2O3) Double Cladding Fiber (*PALYb-03*)

a) Glass fabrication and characterization

In this Section the study and the new process used to the fabrication of glasses for the PALYb-03 fiber is describes. This new method of glass manufacturing has been studied with the aim of reducing the numerical aperture of the core with a precise control on the difference between the refractive index values of the core and the first cladding. This method, named Method 4 (Chapter 3, Section 3.1), consists in preparing a single batch of the core and the first cladding glasses and it is sketched in Figure 4.13.

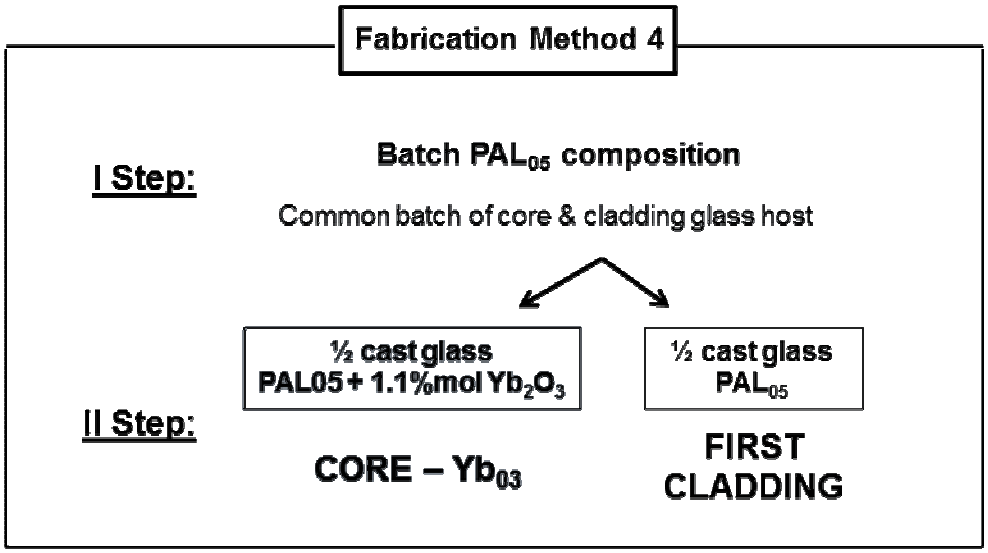

Figure 4.13 – Scheme of the fabrication Method 4

The chemicals of the PAL_{11} composition were weighed (80g) and melted in 'bottom loading' furnace (Proba) in covered alumina crucible. The temperature program was set as follows: the oven was heated up to a temperature of 1350° C for 30 min with a ramp of 10° C/min, then the tempe rature was raised up to 1400° C for 15 min with a rate of 15° C/min. The so-obtai ned glass mass was divided into two parts of equal mass: one for the core glass, the second for the first cladding glass. The core glass part, after grinding, was mixed with 2.6 wt% of Yb_2O_3 (equivalent to 1.1 mol%). The core glass was melted again twice in at 1350℃ for 30' in order to homogenize the glass and to incorporate the ytterbium oxide. The whole process was carried out by blowing 3 l/min of a mixture of dry N_2/O_2 into the furnace. The molten glasses were cast in a pre-heated (400° C) brass plate. The glasses were both annealed at 480° C the glass transition temperature for 5 h. Each glass sample was then cooled down slowly at room temperature. With this method it is possible to control in a precise way the refractive index difference between the core and the first cladding, as the two

glasses coming from the same batch and they have the same fabrication ‘history’.

In Table 4.10 the refractive index values for the prepared samples are reported: Yb_{03} for the core; PAL_{11} for the first cladding. As evidenced by the measures, the values of the refractive index of PAL_{11} are higher compared to PAL_{05}. These two samples have in fact the same nominal composition, but different methods of preparation. The variation of the refractive indices values between these two glasses can be related to the number of melting processes in which PAL_{11} underwent (sample with higher index values). In fact, the higher number of melts may have improved the volatilization of the low molecular weight components from the glass (eg Li_2O), thus resulting in a glass richer in heavy components with a high polarizability.

Table 4.10: Refractive index values for the Yb_{03}, and PAL_{11} samples measured at different wavelengths

Sample	633 nm	825 nm	1016 nm	1316 nm	1533 nm
Yb_{03}	1.596	1.590	1.586	1.582	1.580
PAL_{11}	1.595	1.589	1.585	1.581	1.579

Moreover, with this method it was possible to finely control the refractive index difference between the: core and the first cladding glasses came from the same batch and experienced the same fabrication ‘history’. This control is underlined in Table 4.11, where the refractive index values of two set of samples prepared with Method 4 are reported.

Table 4.11: Refractive index values for the two set of glasses: (Yb_{03}-a, PAL_{11}-a), and (Yb_{03}-b, PAL_{11}-b) samples measured at different wavelengths

λ[nm]	Yb_{03} - a	PAL_{11} - a	Yb_{03} - b	PAL_{11} - b
633	1.5946	1.5936	1.5969	1.5965
825	1.5886	1.5873	1.5904	1.5903
1061	1.5846	1.5833	1.5868	1.5862
1312	1.5811	1.5799	1.5832	1.5827
1533	1.5786	1.5771	1.5804	1.5799

From the values reported in Table 4:11 is evident that the variation of the values of refractive index between core and first cladding is of the order of 10^{-4}. On the basis of the refractive indices measured at 1016 nm, the calculated values of numerical aperture (NA) are equal to 0.06 and 0.04, respectively for the first and second set of samples. With this method of fabrication (Method 4) can be obtained optical fiber with a low numerical aperture in a controlled way. Thus Method 4 allows to fabricate single mode optical fiber with large size of the core. The lifetime of Yb^{3+} ions in the glass Yb_{03} was found to be equal to: (1.4±0.1) ms.

b) Preform fabrication

The manufacture process of the preform followed the same steps as for the previous fibers. The first step was to manufacture the core rod with the composition Yb_{03}. After the annealing, the individual parts of the preform have been systematically cleaned and polished using alumina suspensions of different size, as abrasives, as well as the SiC paper of different grits (from 100 down to 4000). At the end of the polishing process, the different parts of the preform were placed in hot ethanol and subsequently in hot acetone. Particular attention has been done to the cleaning and polishing steps, in order to minimize and eliminate

imperfections or particles on both inner and outer surfaces. To assemble the preform, the core rod was first stretched and fit into the first cladding tube. A second stretch was performed on the core/first cladding structure to reduce its diameter and so it was introduced into the second cladding tube.

c) Fiber drawing and characterization

From the fabricated preform the PALYb-03 fiber was drawn. The dimensions of the PALYb-03 fiber are: (135±1) μm for the diameter of the outer cladding, (50±1) μm for the diameter of the inner cladding and (12±1) μm for the core diameter. Typical values of the drawing process were: a drawing temperature of about 600°C, and drawing speed of 3 m/min.

The calculated V number of the PALYb-03 fiber at 1016 nm is 1.9, which means that the fiber is single mode. An optical micrograph of the fabricated optical fiber cross-section is shown in Figure 4.11(a) where the step-index between the core and the different claddings is evident by the brighter coloration of the center (core) compared to the outer parts of the cross section.

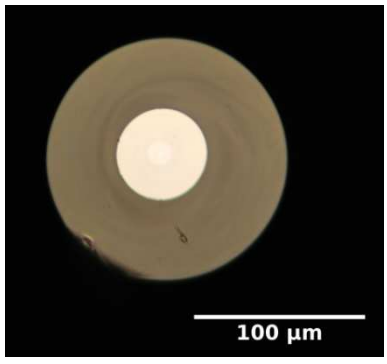

Figure 4.14 - Photograph of the produced PALYb-03 phosphate optical fiber taken by optical microscope

4.6 Optical fiber laser demonstration

A preliminary test to verify the coherent emission Of the produced PALYb-01 and PALYb-02 active fibers were.

Laser performance for the PALYb-01 fiber was demonstrated using 25 mm of this Yb-double cladding fiber. In Figure 4.15, the spectra for lasing operation at maximum available pump power (blue line) and threshold condition (red line) are shown. The laser threshold was for a pump power of 150 mW. The generation of a lasing peak of 15-25 mW with center wavelength at 1022 nm (see Figure 4.14) was observed for a pump power of 248 mW. The bandwidth obtained was 2-3 nm. The laser operation was stable for at least 60 minutes (duration of the experiment). The lasing wavelength remained almost fixed and the output power P_{out} presented fluctuations of the order of 5 dB.

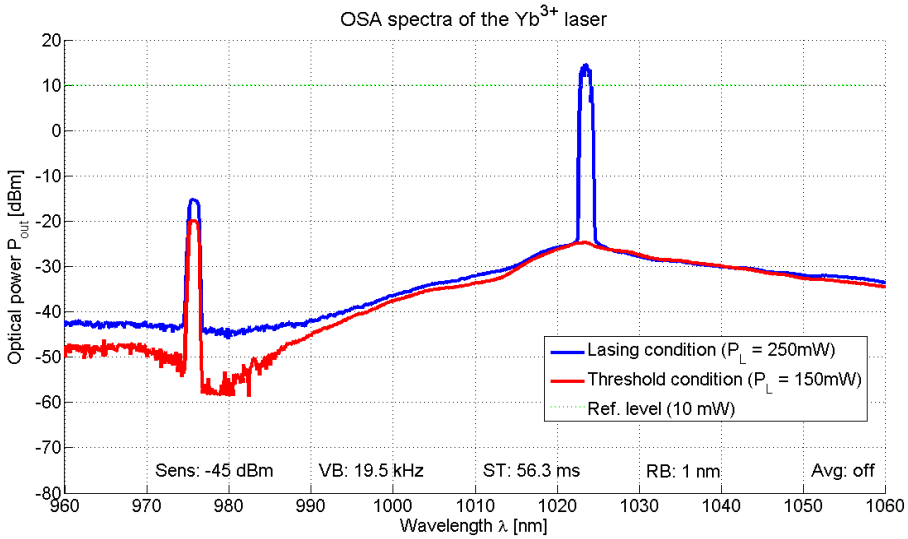

Figure 4.15. Detail of the Yb^{3+} laser output power peak at 1022 nm.

Laser performance for the PALYb-02 fiber was demonstrated using 50 mm of this Yb-double cladding fiber. In Figure 4.16, the spectra for lasing

operation of the PALYb-02 fiber is shown. The maximum output power measured was 5 mW with center wavelength at 1014 nm, for a pump power of 248 mW. The bandwidth obtained was 2-3 nm.

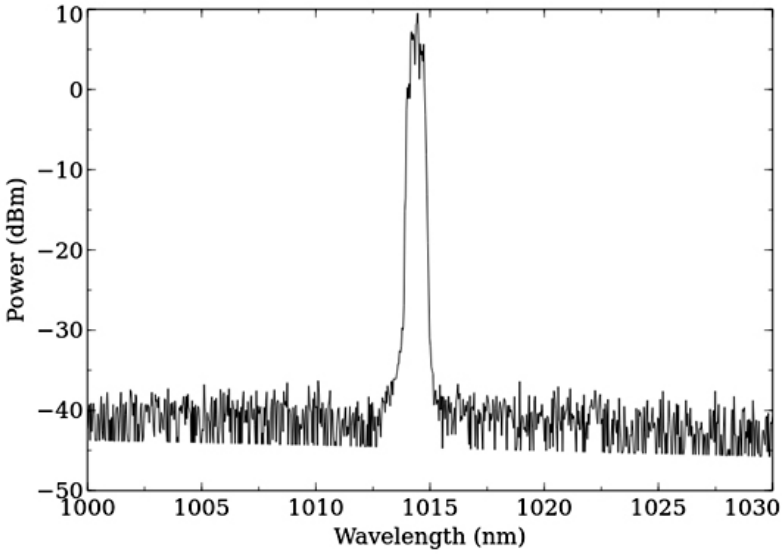

Figure 4.16. Detail of the PALYb-02 laser output power peak at 1014 nm.

Optimal laser performance could have been affected by several factors. Those associated with a non-optimized experimental setup setting could be the following: imperfect alignment between the parts forming the resonance cavity (fiber-guide parallelism, fiber bending, mirror-guide angle), presence of a small gap between the Yb3+-doped fiber and the HR mirror, active fiber end cleaved with an oblique angle or having a bad quality cleaving. In relation with the optical components: the use of a normalized diameter (and NA) would help improving the overall performance of the system. Concerning the WDM: since it is designed to operate with 980 nm and 1060 nm, it could be expected that the power carried at the lasing wavelength (1022 and 1014 nm) splits between the two ports. In this sense it is possible that some amount of the lasing output power reached the pump laser, and consequently, reduced the power available at the system output

(value measured by the OSA). Finally, in relation to the double cladding active fiber: the small distortion and misalignment of the core could lead to coupling losses since the fiber laser was tested using core pumping.

BIBLIOGRAPHY

1. H. Bach, N. Neuroth, The Properties of Optical Glasses, Spinger (1995).
2. T. Harada, H. In, H. Takebe and K. Morinaga, “Effect of B_2O_3 addition on the thermal stability of barium phosphate glasses for optical fiber devices” in *Journal of American Ceramic Society* 87(3), 408-411 (2004).
3. Y. W. Lee, M. J. F. Digonnet, S. Sinha, K. E. Urbanek, R. L. Byer and S. JiangY, “High-power Yb3+-doped phosphate fiber amplifier”, in Journal *of Selected Topics in Quantum Electronics IEEE*, 15(1), 93-102 (2009).
4. X. Zhao, X. Wang, H. Lin, Z. Wang, “Average electronegativity, electronic polarizability and optical basicity of lanthanide oxides for different coordination numbers” in *Physica B Condensed Matter*, 403(1), 1787-1792 (2008).
5. Y. W. Lee, S. Sinha, M. J. F. Digonnet, and R. L. Byer and S. Jiang,“20W single-mode Yb3+-doped phosphate fiber laser” in *Optics Letters*, 31(22), 3255-3257, (2006).
6. D. L. Veasey, D. S. Funk, P. M. Peters, N. A. Sanford, G. E. Obarski, N. Fontaine, M. Young, A. P. Paskin, W. Liu, S. N. Houde-Walter, J. S. Hayden, “Yb/Er-codoped and Yb-doped waveguide lasers in phosphate glass” in *Journal of Non-Crystalline Solids* 263&264, 369-388, (2000).
7. C. Jiang, H. Liu, Q. Zeng, X.Tang and F. Gan, “Yb:phosphate laser glass with high emission cross-section” in *Journal of Physics and Chemistry of Solids* 61(8) 1217–1223 (2000).
8. R. J. Ryder and G. E. Rindone, “Color and Light Scattering of Platinum in Some Lead Glasses” in *Journal of the American Ceramic Society* 41(10), 415–422, (1958).

Chapter 5

Conclusions and Future work

Various phosphate glass compositions were studied and new phosphate optical glasses were design and fabricated. During this research work, it was necessary to explore and study four fabrication process to develop a suitable method of fabrication for phosphate glasses. From the different set of fabricated glasses overall six phosphate fibers were draw: two passive and four doped with Yb_2O_3. A substantial part of the thesis was involved to the implementation and optimization of the rotational casting equipment. To do this, a new rotational casting equipment was designed using Autocad 3D and realized.

The main and most important conclusion of the thesis can be listed as follows:

- A new thermally stable and homogenous phosphate optical glass system was design and fabricated, suitable for fiber drawing.
- Different manufacturing process for phosphate optical glasses were set-up and optimized: controlled refractive index variation to obtain NA=0.05 for the core.
- Core/clad phosphate performs were successfully produced by rod-in-tube technique: rotational casting parameters were optimized for the different cladding compositions, and a custom rotational casting equipment was designed and fabricated.

- Phosphate optical fibers, both active and passive, were fabricated: for the first time with the cladding tubes obtained by rotational casting.
- 2 dB/m: the lowest value of attenuation loss for phosphate fibers.

Innumerable issues were encountered in the various steps of this research work. Thus the different problems, addressed in the study of complex materials such as phosphate glasses for fiber laser applications, and the different solutions proposed and implemented, based on the results observed have been also presented. For draw a final conclusion, the steps of this research work will be summarized below.

The first set of glasses, prepared with Method 1, included: four phosphate glasses with a variable Li_2O/BaO content. The glasses showed high stability against devitrification: the difference between T_g and T_x was found to be higher than 200° C for all samples. The proof-of-concept multimode single cladding optical fiber was drawn (PAL-SC01) from a preform fabricated by the rod-in-tube technique and by using the rotational casting technique to produce the cladding tube. A set up of the rotational casting process was studied and tubes without defects along the length of the preform were obtained. The attenuation loss of the PAL-SC01 fiber was measured to be 7.30 dB/m. The high attenuation loss value is mainly due to scattering effects by small crystallized particles created during the drawing process. The origin of the crystals was related with the high temperatures used during the fabricating process of the performs that caused the incorporation of impurities from the crucibles.

For the second set of phosphate glasses, the attention was then focussed on the design and optimization of the glasses and the process for the fabrication

of the double cladding fiber configuration. Starting for the system previously studied, three phosphate glass compositions were designed and fabricated with the Method 2 for the fabrication of the double-cladding fiber. More than 190° C of difference between the T_x and T_g were found for all three samples. From the studied samples, a double cladding phosphate fiber (PAL-DC01) were drawn the attenuation loss measured was equal to 11.0 dB/m. During the drawing process, a series of scattering centers were evident along the drawn fiber. In fact, the change in the manufacturing parameters (1500° C for only 15 ', instead of 1600° C for 1h as for the previous method) was not enough to solve the problem of crystallization due to impurities. In addition, the values of attenuation losses in the fiber PALDC-01 are related with problems particles, impurities, surface imperfections at different interface of the fiber: core-first cladding and first cladding-second cladding respectively. To improve the performance of the fibers and reduce the attenuation loss, a potential solution was to change manufacturing parameters (further reduction of the temperature and time of glass melting) and an improvement of the quality and repeatability of the cleaning and polishing process of preforms (for both cladding tubes and core rod).

The research work was then focused on the study and fabrication of doped glasses and active fibers. The samples prepared for the active fiber were fabricated by decreasing and adjusting the melting temperature and time of Method 2. A first Yb-doped phosphate double cladding fiber (PAL-Yb01) was drawn with the core doped with a molar concentration of Yb_2O_3 equal to 3.45mol% (8.0 x 10^{20} ion/cm^3). The active fiber PALYb-01 exibited lower values of attenuation loss (7.30 dB/m) than the values of loss of the fiber PALDC-01 but still comparable to the values of losses of the fiber PALSC-01. The scattering

effect in the PAL-Yb01 fiber was even more pronounced in relation to the small dimensions of the core (7 μm).

In order to assess the quality of the PAL-system and exclude intrinsic causes of attenuation loss due to the fabricated materials, a single cladding test fiber, named PAL-test, was drawn and characterized. The preform used for the fabrication of the PAL-test fiber was made from the same glasses used in the PAL-Yb01 fiber. After this test it was pointed out that the very high attenuation loss of the previous PAL-fibers were not related to intrinsic problems of the material. In fact, even if composed of the same glasses, the attenuation loss of the PAL-test fiber (2.0 dB/m) were lower than the values of the previous PALYb-01 fiber. In addition, the PAL-test fiber presented attenuation losses values far lower than PALSC-01, with which it shares the same dimensions but different manufacturing processes and so different glasses. As a result the changes and the adjustment occurred during this work in the manufacturing process of glass and preform led to an improvement of the fabricated glasses and of the performance of the produced fibers.

After this test, a different method of fabricating phosphate glass samples was investigated in order to improve the quality and the reproducibility of the glass in terms of refractive index variations. A second active fiber PALYb-02 was drawn and characterized with the set of glasses obtained from this method: Method 3. In particular, the glass-former P_2O_5 was replaced by the precursor $NH_4H_2PO_4$.This change has been made to have better control in the weighing process of chemicals and to minimize contamination by moisture present in the atmosphere. It was noted, however, that different samples prepared by Method 3 showed a slight yellow/brown coloring, probably due to contamination of the

platinum crucible (coloration not shown systematically by all the different glasses prepared with this method). The high contamination of Pt can be derived from the presence of ammonia coming from the first fusion of the precursor. Nevertheless, the PALYb-02 fiber was drawn as a test for the fabrication method. The attenuation loss values of the PAL-Yb02 were relative high (18.2 dB/m) compared to the values of the previous fibers. This suggest problems resulting from the new fabrication process combined with the new precursor. Although this process has led to a better control on the variations of the refractive index, Method 3, with the precursor $NH_4H_2PO_4$, leads to the fabrication of glasses not suitable for the use as optical fibers.

A new method (Method 4) was then studied and developed with the aim of reducing the NA of the core by precisely controlling the refractive index variation between the core and the first cladding. With this method it was possible to finely control the refractive index difference between the core and the first cladding: the variation of the values of refractive index between core and first cladding is of the order of 10^{-4}. The NA values for the prepared glass were in the order of 0.05. Thus with this method it was possible to fabricate a single mode phosphate fiber (PAL-Yb03) with a µm core.

In the contest of the research group, laser emission of the fabricated fibers (PAL-Yb01 and PAL-Yb02) was also demonstrated at the end of the this work.

This thesis should be seen as a starting work on the phosphate glasses and phosphate glass fibers. Further studies can be carried out and developed regarding the material and the laser set-up.

As regard the material, additional study can be focus on the optimization of the composition. In particular, the reduction or the complete elimination of the alkali metal oxides (Li_2O) could lead to a further increase of the chemical stability, reducing the hygroscopicity, and mechanical strength of the phosphate glasses. Furthermore, reducing the content of lead oxide could be interesting to decrease the non-linear refractive index, and in general it might be interesting also to decrease the refractive index of the PAL-glasses, in view of splicing the PAL-fibers with the commercial fibers.

For what concern the laser set up, in future study would be necessary to test the PAL-fibers in cladding pump mode and then take full advantages of the double cladding configuration. Moreover, laser test should investigate the performance of the PAL-fibers as active cavity in pulsed laser systems.